



UNIVERSITY OF LEEDS

This is a repository copy of *Agglomeration dynamics in liquid–solid particle-laden turbulent channel flows using an energy-based deterministic approach*.

White Rose Research Online URL for this paper:
<http://eprints.whiterose.ac.uk/160365/>

Version: Accepted Version

Article:

Mortimer, LF, Njobuenwu, DO orcid.org/0000-0001-6606-1912 and Fairweather, M (2020) Agglomeration dynamics in liquid–solid particle-laden turbulent channel flows using an energy-based deterministic approach. *Physics of Fluids*, 32 (4). 043301. ISSN 1070-6631

<https://doi.org/10.1063/5.0001596>

© 2020 Author(s). This is an author produced version of an article published in *Physics of Fluids*. Uploaded in accordance with the publisher's self-archiving policy.

Reuse

Items deposited in White Rose Research Online are protected by copyright, with all rights reserved unless indicated otherwise. They may be downloaded and/or printed for private study, or other acts as permitted by national copyright laws. The publisher or other rights holders may allow further reproduction and re-use of the full text version. This is indicated by the licence information on the White Rose Research Online record for the item.

Takedown

If you consider content in White Rose Research Online to be in breach of UK law, please notify us by emailing eprints@whiterose.ac.uk including the URL of the record and the reason for the withdrawal request.



eprints@whiterose.ac.uk
<https://eprints.whiterose.ac.uk/>

Agglomeration dynamics in liquid-solid particle-laden turbulent channel flows using an energy-based deterministic approach

L. F. Mortimer^{a)}, D. O. Njobuenwu, and M. Fairweather

School of Chemical and Process Engineering, University of Leeds, Leeds, LS2 9JT, UK

^{a)} *Corresponding author: l.f.mortimer@leeds.ac.uk*

A deterministic particle-particle agglomeration technique is applied together with direct numerical simulation and four-way coupled Lagrangian particle tracking in order to accurately simulate and investigate fully-coupled agglomerating particle-laden channel flows at shear Reynolds number, $Re_\tau = 180$. The collision outcome determination (recoil or aggregate) is based upon the balance between kinetic energy dispersed in the collision and the work required to overcome the van der Waals attractive potential. The influence of particle size ($d_p = 202, 286$ and $405 \mu\text{m}$), both at fixed volume fraction ($\phi_p = 10^{-3}$) and fixed primary injected particle number ($N_p = 109,313$), on the resulting collision and agglomeration dynamics is investigated. Attention is also focused on how collision and agglomeration rates vary throughout the wall-normal regions of the channel flow. The results demonstrate that normalized collision rates are similar for all particle sizes at fixed volume fraction, but increase with particle size at fixed particle number, and a preference is observed for collisions to occur close to the walls. Despite this, in all cases considered here, agglomeration events are most frequent at the centre of the channel, with agglomeration efficiencies also peaking in this region. In terms of particle diameter effects, the smallest particles exhibit the greatest preference to aggregate, given a collision has already occurred. Furthermore, whereas normalized collision and agglomeration event counts show differing diameter-dependence based on whether the number of primary particles or the volume fraction is fixed, agglomeration rates show diameter-independence and as such are based on solely particle size and local dispersive properties. Analysis of the dynamic collision properties throughout the channel confirms that agglomeration is favoured within the bulk flow region due to low relative particle velocities and small collision angles at this location. The temporal evolution of important interaction properties is investigated, all of which demonstrate stability over the course of the time simulated. Particle diameter is also shown to influence the long-term population of higher-order agglomerates, with (for a given volume fraction) smaller particles aggregating faster to form larger particles. The systems studied, which resemble those present in the processing of nuclear waste, all exhibit substantial agglomeration over the time considered. This reinforces the importance of accurately modelling agglomeration dynamics in flows where electrokinetic interactions are important, in order to correctly predict multiphase flow properties over long timeframes.

I. INTRODUCTION

Dense, interacting particle-laden flows are practically relevant in many natural and industrial processes. For instance, mineral processing (Guha et al., 2007), atmospheric transport (Folini et al., 2008) and blood drop forensics (Chen et al., 2016) are just a few research fields where understanding surrounding both the particle-scale and system-scale dynamics is essential to determining the long-term behaviour of the flow. Of particular relevance to this work, the nuclear industry relies on scientific understanding of particulate flow properties within waste suspension flows (Chun et al., 2011). For instance, a key challenge exists in the transportation of legacy nuclear waste material from historic storage ponds and silos to interim locations where they are to be safely stored. Generation of knowledge of the particle collision, aggregation and interaction dynamics in these systems is currently of increasing importance, and the ability to predict the long-term morphology of the particles (size, shape and interaction profiles at long flow times) is necessary to foresee potential processing problems or issues in future and present waste transport system designs. This work focuses on generating knowledge surrounding multiphase flows with high particle-fluid volume fractions. In such densely dispersed flows, particles are often capable of agglomerating with each other due to electrokinetic interactions (Krozel, 1994), forming larger particulate structures which can result in blockages, poor heat-transfer conditions and regions of local concentration increase. The latter also contributes to carrier fluid-turbulence modulation (Kussin and Sommerfeld, 2002), which can then impact further on transport efficiency. The ability to predict system-specific properties such as agglomeration efficiencies and particle flow rates is also of use in many other practical applications (Shook and Roco), but as of yet we are currently without a model capable of doing so accurately, and specifically a model that fully accounts for the micro-scale particle-particle interactions which determine the outcome of a collision (recoil or agglomeration).

Despite the challenges, recent advances in computational performance have allowed direct numerical simulation (DNS) to grow into an important and useful tool in the study of particle-laden turbulent flows. Since it is nearly impossible to measure individual particle-particle interactions experimentally with current technology, various types of computational fluid dynamics model are fast becoming the sole means of studying such phenomena. However, given that there exists a lack of experimental data to validate such models against, it is necessary to rely on first principles, high fidelity computational tools to develop fundamental understanding of the important processes that underpin such flows. In this sense, we are restricted to assessing the veracity of new findings through comparison with previous work and qualitative analysis to determine the plausibility of any results, and so it is of utmost importance that we use high accuracy computational techniques when attempting to simulate such systems.

Previous work carried out in dilute flow regimes has aided greatly in the identification and understanding of some of the key dispersive features of particle-laden turbulent flows. One-way coupled simulations indicate that two mechanisms are

responsible for particle migration and local concentration increases, these being preferential accumulation and turbophoresis. Computational studies (Elghobashi and Truesdell, 2006; Squires and Eaton, 1991; Eaton and Fessler, 1994) indicate that preferential accumulation is greatest at around $St_\eta \approx O(1)$, where St_η is the Stokes number based on the Kolmogorov timescale. In this regime, particles are observed to gather in regions of low velocity magnitude, and this has also been confirmed experimentally (Fessler et al., 1994). Turbophoresis refers to the tendency for particles to migrate toward regions of low turbulence kinetic energy, again observed to magnitudinally scale with Stokes number (Kuerten and Vreman, 2005; Marchioli et al., 2008; Marchioli and Soldati, 2002). Upon reaching the wall regions, particles interact with local turbulence structures and show a wide variety of behaviours based on their inertial properties (Mortimer et al., 2019).

Extensive work has been performed in the one-way coupled regime, but if the volume fraction of particles in a turbulent flow, ϕ_p , is increased and the system is no longer dilute ($\phi_p > 0.001\%$), the influence of the particles' momentum feedback to the turbulence must also be taken into account (Eaton, 2009). It is widely established by many studies in both wall-bounded, channel flows (Pan and Banerjee, 1996) and isotropic turbulence (Boivin et al., 1998) that large particles enhance the turbulence whereas small particles attenuate it. However, this effect has been shown to be less pronounced for systems with low density ratios, despite having equivalent Stokes numbers (Lucci et al., 2011). Since the present work is of relevance to liquid-solid flows where electrokinetic forces are significant, analysis of the type carried out by the latter authors is brief, and since we are interested in industrial liquid-solid flows, the particle-fluid density ratio is fixed at $\rho_p^* = 2.71$ (although two-way coupling effects in the calculations are included for accuracy and confirmation of negligible effects).

In high volume fraction ($\phi_p > 0.1\%$) liquid-solid and gas-solid suspensions, particle motion is governed by both hydrodynamic and particle-particle interactions, as indicated by the phase diagram of (Elghobashi, 1994). In this regime, prediction of the resulting particle behaviour is challenging, but various methods of simulating such multiscale/multiphase systems have been attempted in recent years. The main obstacle is in resolving the issue of binary collision detection, with algorithms such as nearest-neighbour lists (Hoomans et al., 1996) or stochastic models (Oesterle and Petitjean, 1993; Sommerfeld, 2001) being the primary methods of doing so. For this work, we adopt a computationally efficient and accurate deterministic collision detection algorithm, as detailed by (Chen et al., 1999), using the hard-sphere model to calculate resultant positions and velocities post-collision.

Four-way coupled simulations of particle-laden systems have also been performed in recent years (Vreman et al., 2009; Zhao et al., 2015; Laín et al., 2002). Ireland et al. (2016) studied the preferential concentration of colliding inertial particles in isotropic turbulence, determining that particles with low Stokes numbers preferentially accumulate in regions of irrotational

dissipation due to vortex ejection mechanisms. It was also determined that relative particle collision velocity statistics are weakly sensitive to changes in Reynolds number, particularly for low St_η .

Work on post-collision effects such as particle agglomeration in turbulent flows is sparse, despite most real liquid-solid flow systems being affected by electrokinetic interaction dynamics. The most common interactions are that the particles either bounce off one-another, or that they stick together (adhesion) forming an ‘agglomerate’ (Henry et al., 2013). Schutte et al. (2015) studied the effects of a ‘hit and stick’ agglomeration model to examine particle aggregation, breakup, deposition and re-entrainment in turbulent channel flows. It was observed that both large eddy simulation (LES) and DNS results indicated similar behaviour, and that two-way coupling had an effect on the characteristics of the agglomerates.

In most flows, the adhesion efficiency of particles with other particles, unlike with droplets (Charalampous and Hardalupas, 2017), is usually much less than one. The determination of particle-particle aggregation can be based on various approaches to modelling the dynamics of the collision (Wang et al., 2015). These are divided into three main categories. The first are energy-based models (Alletto, 2014) which determine agglomeration based on whether the dissipated energy in a collision is sufficient to trap the particles in the van der Waals attraction zone. There are also momentum-based models (Balakin et al., 2012; Kosinski and Hoffmann, 2011) in which adhesion and elastic repulsion forces are compared at the moment of impact to determine the outcome of agglomeration. Finally, the DLVO forces can be calculated explicitly (Fujita and Yamaguchi, 2007; Choi and Djilali, 2016), which has proven useful for nano-scale suspensions or laminar flows, but requires much more computational effort due to DLVO theory’s associated very small timescales. Other simpler flow regimes such as magnetic suspensions in creeping flow (Roure and Cunha, 2018) and homogeneous turbulence (Dizaji and Marshall, 2016) have been studied in recent years, however the effects due to the diverse nature of turbulent structures within the channel flow are yet to be fully understood.

The present work adopts and expands upon the energy-based particle-particle agglomeration model with a hard-sphere collision and detection algorithm which has previously been successfully applied to the LES of turbulent channel flows studying inertial fibres, agglomeration and breakup (Njobuenwu and Fairweather, 2015, 2017, 2018). The aggregation process considers the surface-level electrokinetic interaction, but the particles are assumed to have zero net charge in line with DLVO theory. As such, particle-particle electrokinetic interaction calculations are not required. By switching to a DNS continuous phase solver, we aim here to provide a much more accurate representation of the fundamental dynamics which underpin particle-particle interaction in various regions of turbulence, which differ throughout the channel flow and have not been discussed in previous studies in this field. More specifically, correct interparticle collision detection and resolution relies on accurate representations of the local velocity field, which for trajectories smaller than the cut-off filter are inaccurate in the case of LES. This has consequences for particle collision angles and hence the kinetic energy of the collisions which is important in determining

agglomeration efficiency. To relate the work to real nuclear waste flows, we will consider various sizes of spherical calcite (Vdović and Bišćan, 1998) particles in water, with calcite frequently employed as a simulant for nuclear waste material. The focus of the present work is to generate understanding in regards to the key solid phase properties, such as particle concentration and diameter, which lead to successful agglomeration events. Since particle volume fraction can be increased by modification of either of these parameters, the effect of variations of each shall be considered separately. Furthermore, we aim to improve the present understanding of agglomerating solid-liquid flows, which are often quantified by solely bulk properties, by analysing interaction dynamics based on local dispersive properties of the particulate phase. Hence, this work will also focus on correlating particle dynamics in the various wall-normal regions of the channel flow with the collision and agglomeration behaviour observed in those zones.

II. METHODOLOGY

A. Single-phase channel flow simulation

The direct numerical simulation (DNS) code, Nek5000 (Fischer et al., 2008), is employed to generate high accuracy predictions of the flow field which resolves all of the relevant turbulence length and timescales. The Eulerian solver utilizes a high-order ($N = 7$) spectral element method in order to simulate the fluid phase in a turbulent channel flow at shear Reynolds number, $Re_\tau = u_\tau \delta / \nu_F = 180$. Here, u_τ is the shear velocity, δ is the channel half-height and ν_F is the fluid kinematic viscosity. This code was chosen due to its efficient parallelisation capabilities and extensive validation history. The open-source solver is also a suitable framework ideal for developing additional components. The governing equations associated with the continuous phase dynamics are the dimensionless incompressible continuity and Navier-Stokes equations, given by:

$$\nabla \cdot \mathbf{u}_F^* = 0, \quad (1)$$

$$\frac{D\mathbf{u}_F^*}{Dt^*} = -\nabla p^* + \frac{1}{Re_B} \nabla^2 \mathbf{u}_F^* + \mathbf{f}_{PG}^* + \mathbf{f}_{2W}^*, \quad (2)$$

where $\mathbf{u}_F^*(\mathbf{x}^*, t^*)$ is the fluid velocity vector at position \mathbf{x}^* and time, t^* , $p^*(\mathbf{x}, t)$ is the fluid pressure, Re_B is the bulk Reynolds number defined as $Re_B = U_B \delta / \nu_F$ and \mathbf{f}_{PG}^* represents the constant pressure gradient forcing term. The above equations have been non-dimensionalised using the channel half-height, δ , the bulk velocity, U_B , and the fluid phase density, ρ_F . Henceforth, any parameter or quantity labelled with an asterisk (*) denotes a non-dimensionalised variable obtained using these bulk properties (δ, U_B, ρ_F). The additional term \mathbf{f}_{2W}^* accounts for the total two-way momentum exchange between particles in the corresponding cell and the surrounding fluid, details of which will be provided in the following subsection.

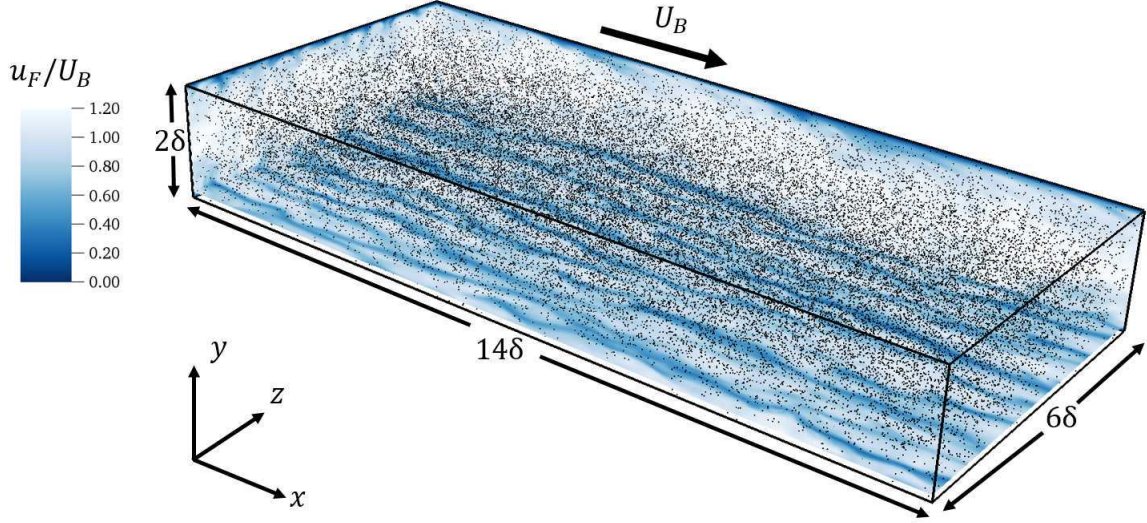


Figure 1: Schematic of the multiphase turbulent channel flow at $Re_\tau = 180$. Colour indicates fluid velocity magnitude non-dimensionalised by the bulk flow velocity, U_B . Black spheres indicate locations of particles.

The conservation equations are solved on a discretized structured Cartesian grid which consists of $27 \times 18 \times 23$ 7th-order spectral elements (i.e. 3.9M nodes). These are scaled in the wall-normal direction of the channel such that those closest to the wall are thinner and more compactly distributed. Elements are uniformly distributed in the streamwise and wall-normal directions. The computational domain (x, y, z) has a size $14\delta \times 2\delta \times 6\delta$, representing the channel, with boundaries chosen to ensure all vortical structures are captured. This is illustrated in the Figure 1. Here, x refers to the streamwise direction, y refers to the wall-normal direction, and z refers to the spanwise direction. Periodic boundary conditions are enforced at both limits of the streamwise and spanwise axes, whereas the wall-normal axis enforces no-slip and impermeability conditions at $y^* = \pm 1$. The flow is driven and maintained by a constant pressure gradient throughout the streamwise (x) direction, which has magnitude:

$$\frac{\partial p^*}{\partial x^*} = \left(\frac{Re_\tau}{Re_B}\right)^2. \quad (3)$$

As already noted, $Re_\tau = u_\tau \delta / \nu_F$ represents the shear Reynolds number, with $u_\tau = \sqrt{\tau_W / \rho_F}$ the shear velocity and τ_W the mean shear stress at the wall boundary. The continuous phase parameters for the single-phase predictions of the turbulent channel flow at $Re_\tau = 180$ are presented in Table 1. The solver uses a constant timestep $\Delta t^* = 0.005$ and is initialized with a laminar profile containing minor perturbations in the off-stream directions in order to encourage the transition to turbulence. First- and second-order flow statistics were monitored in order to determine convergence to a statistically stationary state before further statistics were gathered for validation and analysis purposes.

Table 1: Parameters for DNS of turbulent channel flow. $L_{x,y,z}$ represent the Cartesian lengths of the domain, $E_{x,y,z}$ are the number of elements in each direction.

Re_τ	Re_B	$L_x \times L_y \times L_z$	$E_x \times E_y \times E_z$	Δt^*
180	2800	$14\delta \times 2\delta \times 6\delta$	$27 \times 18 \times 23$	0.005

B. Lagrangian particle tracking

A Lagrangian particle tracking (LPT) routine was developed in order to calculate the trajectories of the solid particles through the flow, which interfaces concurrently with Nek5000. Each discrete element of the particle ensemble is represented by a point-like, impenetrable, undeformable computational sphere. Upon performing a continuous-phase timestep, the LPT solves the non-dimensional equations of motion for each particle in the system. The Newtonian acceleration and velocity differential equations are derived by considering the force-balance between the particle's inertia and the fluid (Maxey, 1987; Riley and Patterson Jr, 1974). Within this study, we consider a calcite-water system wherein the density ratio is low ($\rho_p^* = 2.71$) and, as such, contributions from forces other than drag are likely to be relevant, as observed previously (Homann and Bec, 2010; Mortimer et al., 2019). For this reason, we have chosen to consider contributions from all hydrodynamic forces (drag, lift, virtual mass and pressure gradient). The relevance of all these forces based upon channel wall-distance can be found in Mortimer et al. (2019). The Basset history force has been neglected due to long computation times and previous evidence demonstrating little effect on the resulting particle motion (Fairweather and Hurn, 2008; Daitche, 2015). Furthermore, gravitational and buoyancy forces were neglected for two reasons: firstly, the focus of the present work is on understanding the effects of turbulence on particle-particle interaction and agglomeration, the emergent behaviour of which is still not fully studied or comprehended, and hence it would be difficult to isolate effects solely turbulence-based. Furthermore, a secondary aim is to compare the present findings consistently to similar studies which also did not take into account gravitational effects. The equations of motion solved for each solid element are as follows:

$$\frac{\partial \mathbf{x}_p^*}{\partial t^*} = \mathbf{u}_p^*, \quad (4)$$

$$\frac{\partial \mathbf{u}_p^*}{\partial t^*} = \frac{1}{M_{VM}} \left[\underbrace{\frac{3C_D |\mathbf{u}_s^*|}{4d_p^* \rho_p^*} \mathbf{u}_s^*}_{\text{Drag}} + \underbrace{\frac{3C_L}{4\rho_p^*} (\mathbf{u}_s^* \times \boldsymbol{\omega}_f^*)}_{\text{Lift}} + \underbrace{\frac{1}{2\rho_p^*} \frac{D\mathbf{u}_f^*}{Dt^*}}_{\text{Virtual Mass}} + \underbrace{\frac{1}{\rho_p^*} \frac{D\mathbf{u}_f^*}{Dt^*}}_{\text{Pressure Gradient}} \right]. \quad (5)$$

{Daitche, 2015 #230} {Daitche, 2015 #230} In Eqs. (4) and (5), \mathbf{x}_p^* represents the particle position vector, \mathbf{u}_p^* is the particle velocity vector, \mathbf{u}_f^* is the fluid velocity vector at the position of the particle, $\mathbf{u}_s^* = \mathbf{u}_f^* - \mathbf{u}_p^*$ is the slip velocity between the fluid and the particle, d_p^* is the particle diameter non-dimensionalised by the channel half-height, ρ_p^* is the density ratio between the fluid and the particle and $\boldsymbol{\omega}_f^*$ is the vorticity of the fluid at the particle position, given by $\boldsymbol{\omega}_f^* = \nabla \times \mathbf{u}_f^*$. Further details surrounding the calculation and origin of these terms are provided in Mortimer et al. (2019).

Particle motion is calculated after completion of a fluid timestep. First, through spectral interpolation we obtain the fluid velocity and derivative fields. Eqs. (4) and (5) are integrated using a fourth order accuracy Runge-Kutta scheme (with a Δt^* equal to that of the continuous phase solver) in order to obtain each particle's new position and velocity. Once completed for all particles in the channel, the collision detection and agglomeration determination/resolution algorithm is run, as detailed later. Particle-wall interactions are also detected and resolved using elastic collisions, with the particle wall-normal velocity simply reflected upon colliding with the channel wall. In the periodic directions (streamwise and spanwise), particles which leave the boundary are reinjected to the corresponding location at the other side of the domain, adhering to the periodic nature of the channel flow. For increased volume fractions, the hydrodynamic forces exerted by the dispersed phase onto the carrier fluid must be modelled to ensure accuracy. Each particle's inertial effect on the fluid phase is considered through the inclusion of an additional source term in the Navier-Stokes equations, commonly referred to in the literature as the particle-source-in-cell method (Zhao et al., 2015). The acceleration term in the Navier-Stokes equations applied to cell i is given by:

$$f_{2W}^{*i} = \frac{1}{V_i^*} \sum_j^{N_{p,i}} \frac{\partial \mathbf{u}_{p_j}^*}{\partial t^*}, \quad (6)$$

where V_i^* is the volume of the computational cell and j is an index which iterates over the number of particles contained within that cell, $N_{p,i}$.

The LPT also considers deterministic particle-particle interactions (or four-way coupling) in the form of hard-sphere elastic collisions in order to more accurately simulate systems with increased solid-phase volume fractions, $\phi_p \geq 10^{-3}$. Here, we choose to adopt the hard-sphere collision model, a technique which assumes that the particle collision contact time is much smaller than the LPT integration timestep, which is realistic when the particles are rigid and undeformable. Associated assumptions are that the transfer of rotational momentum is negligible and all collisions are frictionless.

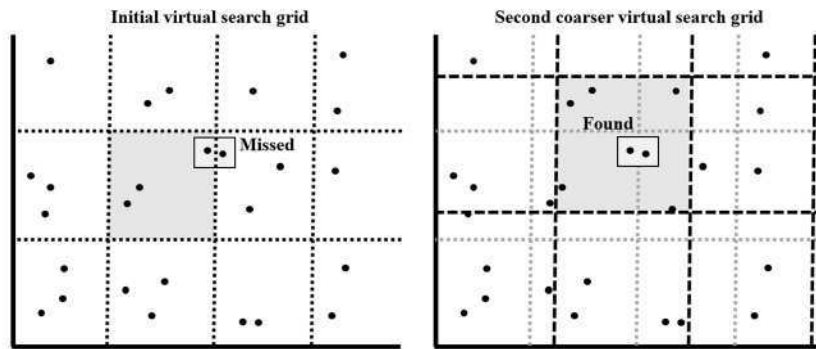


Figure 2: Initial (left) and secondary (right) search grids for deterministic binary collision identification.

Furthermore, we assume that any other interparticle forces acting over the course of the collision are negligible, or in the case of agglomeration are modelled separately. Finally, we assume all collisions are binary, such that tertiary or larger collision

events are sufficiently rare that the resolution of such would improve the accuracy only minimally. To improve computation times, a deterministic binary collision search algorithm, based on the work of Breuer and Almohammed (2015), is implemented.

At each timestep, the particles are distributed into cells within a secondary coarse mesh, with the number of cells specified by the user. This is illustrated in the left hand diagram of Figure 2. The collision algorithm is then performed on each individual cell in this new mesh, treating each as a new full domain. The code determines which particles have collided by checking their relative inter-surface displacements and velocities. If both quantities are below zero, the particles collide. This algorithm is performed on all cells and allows for fast collision detection, reducing the computation time order from $O(N_P^2)$ to $O(N_P)$. The search is then repeated on a slightly coarser grid (right hand diagram of Figure 2), identifying pairs of particles which might have been missed in the initial search. In all simulations considered within the present work we chose a value of 32^3 equal cells for the initial search and 30^3 cells for the secondary search, which provided the fastest computational times whilst ensuring the initial boxes were large enough to capture most of the collisions. It is important to note that without an algorithm such as this, accurate collision identification for large particle numbers would be close to impossible with current computational resources. To perform the collision, standard hard-sphere kinetic energy and momentum conservation arguments are used, as in similar previous models (Yamamoto et al., 2001; Chen et al., 1999), to determine resultant velocities.

A deterministic particle agglomeration model has also been implemented in the LPT code to predict aggregation events upon particle collisions. The responsible interaction in related multiphase waste transport flows for particle cohesion is that due to van der Waals attractive forces (Tingey et al., 1999). The model, based upon the energy-based arguments presented by (Almohammed and Breuer, 2016), and implemented for an LES solver in Njobuenwu and Fairweather (2017), determines that particle agglomeration occurs if the kinetic energy remaining after it is dissipated during the particle collision compression period is such that it is insufficient to provide the work necessary to overcome the van der Waals potential energy. Here it is assumed that the particles possess zero net charge, and that all electrokinetic interactions take place close to the surface of the particle. This model provides an alternate means to having to explicitly calculate the two interaction force components, due to the DLVO range being much smaller than the typical hydrodynamic distance. The requirement for a successful agglomeration event upon collision is such that:

$$\mathbf{u}_{p,r}^{*2} - \frac{(1 - e_n^{*2})(\mathbf{u}_{p,r}^* \cdot \hat{\mathbf{n}})^2}{|(\mathbf{u}_{p,r}^* \cdot \hat{\mathbf{n}})|} \leq \frac{H^*}{6\delta_0^{*2}} \left[\frac{6(1 - e_n^{*2})}{\pi^2 \rho_p^* \bar{\sigma}^*} \left(\frac{d_{p,1}^{*3} + d_{p,2}^{*3}}{d_{p,1}^{*2} d_{p,2}^{*2} (d_{p,1}^* + d_{p,2}^*)} \right) \right]^{\frac{1}{2}}, \quad (7)$$

where $\mathbf{u}_{p,r}^*$ is the relative particle collision velocity (as illustrated in Figure 3), e_n^* is the coefficient of normal restitution, H^* is the non-dimensional Hamaker constant such that $H^* = H/\rho_F U_B^2 \delta^3$, $\bar{\sigma}^* = \bar{\sigma}/\rho_F U_B^2$ is the non-dimensional yield pressure and $\delta_0^* = \delta_0/\delta$ is the minimum contact distance.

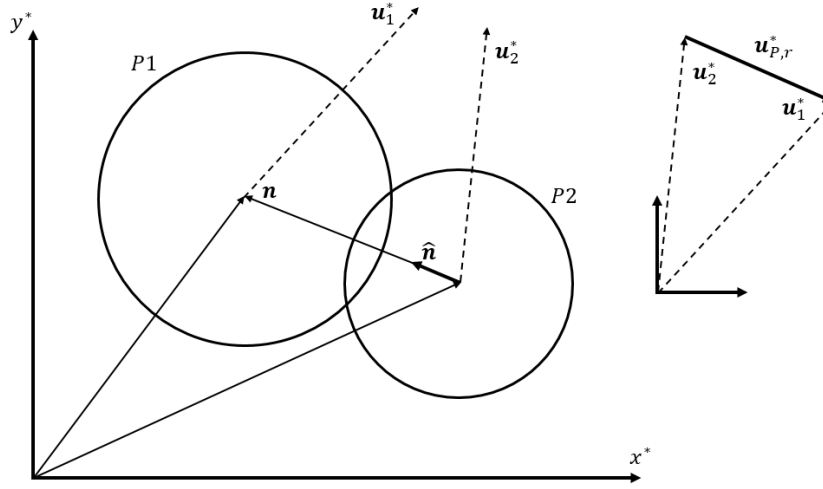


Figure 3: Collision detection schematic. Note that particle overlap is greatly exaggerated for clarity. Top-right: illustration of relative velocity vector calculation, $\mathbf{u}_{p,r}^* = \mathbf{u}_1^* - \mathbf{u}_2^*$.

The unit vector $\hat{\mathbf{n}}$ points from particle 2 (P2 in Figure 3) to particle 1 (P1). If the above Eq. (7) requirement is met, then the two particles form a new spherical particle with a total volume based on the sum of the volumes of the two original particles. The agglomerate is then assigned the following velocity, \mathbf{u}_{agg}^* , and position, \mathbf{r}_{agg}^* , which derive from momentum conservation arguments:

$$\mathbf{u}_{agg}^* = \frac{1}{d_{agg}^*} (d_{p,1}^{*3} \mathbf{u}_1^* + d_{p,2}^{*3} \mathbf{u}_2^*), \quad (8)$$

$$\mathbf{x}_{agg}^* = \frac{1}{2} (\mathbf{x}_1^* + \mathbf{x}_2^*) + t_{col} \mathbf{u}_{agg}^*, \quad (9)$$

where d_{agg}^* is the non-dimensional diameter of the resulting agglomerate given by:

$$d_{agg}^* = \sqrt[3]{d_{p,1}^{*3} + d_{p,2}^{*3}}. \quad (10)$$

The additional terms are as follows: $d_{p,1}^*$ and $d_{p,2}^*$ are the non-dimensional diameter of the first and second colliding particles, respectively, \mathbf{u}_1^* and \mathbf{u}_2^* are the collision velocities, \mathbf{x}_1^* and \mathbf{x}_2^* are the collider positions and t_{col} is the collision overlap time, calculated using the overlap distance and relative particle velocity.

Particles in multiphase flows are characterized by their Stokes number. This is a measure of the particle response timescale to a sensible system-specific fluid timescale, such as the bulk timescale, $\tau_{FB} = \delta/U_B$, or the shear/viscous timescale, $\tau_{FV} = \nu_F/u_\tau^2$. As such, the bulk and shear/viscous Stokes numbers for a particle are given by $St_B = \tau_p/\tau_{FB}$ and $St^+ = \tau_p^+ = \tau_p/\tau_{FV}$, respectively, where τ_p is the particle relaxation time, given by $\tau_p = \rho_p^* d_p^{*2}/18\nu_F$. In the present work, the Stokes number is varied by modifying the particle diameter.

Table 2: Particle-phase parameters for fixed volume fraction (FVF) and fixed particle number (FPN) multiphase turbulent flow simulations at $Re_\tau = 180$.

Parameter	St ⁺ 0.5 FVF	St ⁺ 0.5 FPN	St ⁺ 1 FVF/FPN	St ⁺ 2 FVF	St ⁺ 2 FPN	Units
St^+	0.5	0.5	1	2	2	-
St^*	0.043	0.043	0.086	0.173	0.173	-
τ_P	6.17	6.17	12.35	24.7	24.7	ms
ρ_P	2710	2710	2710	2710	2710	kg m ⁻³
ρ_P^*	2.71	2.71	2.71	2.71	2.71	-
d_P	202.5	202.5	286.4	405.0	405.0	μm
d_P^*	0.0101	0.0101	0.0143	0.0202	0.0202	-
d_P^+	1.82	1.82	2.58	3.64	3.64	-
Θ_P	10 ⁻³	3×10 ⁻⁴	10 ⁻³	10 ⁻³	3×10 ⁻³	-
N_P	309,185	109,313	109,313	38,468	109,313	-
Δt^*	0.005	0.005	0.005	0.005	0.005	-
Δt^+	0.06	0.06	0.06	0.06	0.06	-
A	3.8 × 10 ⁻²⁰	3.8 × 10 ⁻²⁰	3.8 × 10 ⁻²⁰	3.8 × 10 ⁻²⁰	3.8 × 10 ⁻²⁰	J
A^*	2.42 × 10 ⁻¹⁶	2.42 × 10 ⁻¹⁶	2.42 × 10 ⁻¹⁶	2.42 × 10 ⁻¹⁶	2.42 × 10 ⁻¹⁶	-
δ_0	2.0 × 10 ⁻¹⁰	2.0 × 10 ⁻¹⁰	2.0 × 10 ⁻¹⁰	2.0 × 10 ⁻¹⁰	2.0 × 10 ⁻¹⁰	m
δ_0^*	1.0 × 10 ⁻⁸	1.0 × 10 ⁻⁸	1.0 × 10 ⁻⁸	1.0 × 10 ⁻⁸	1.0 × 10 ⁻⁸	-
$\bar{\sigma}$	3.0 × 10 ⁸	3.0 × 10 ⁸	3.0 × 10 ⁸	3.0 × 10 ⁸	3.0 × 10 ⁸	Pa
$\bar{\sigma}^*$	0.15 × 10 ⁸	0.15 × 10 ⁸	0.15 × 10 ⁸	0.15 × 10 ⁸	0.15 × 10 ⁸	-
e_N	0.4	0.4	0.4	0.4	0.4	-

III. RESULTS AND DISCUSSION

A. Continuous phase flow validation

An initial unladen simulation was performed in order to establish statistically stationary turbulence at $Re_\tau = 180$. An initial flow field was provided with a similar fluid mean velocity profile to that expected, along with small perturbations in order to provide enough initial turbulence kinetic energy for the transition to turbulence. First- and second-order velocity statistics were monitored at intervals every $t^* = 100$ until no variation with time was observed. The statistics were then cleared, and the timer was reset. New velocities and relevant derivative variables were sampled over the time period $0 \leq t^* \leq 300$. Plotted in Figure 4 are the mean streamwise fluid velocity and root-mean-square velocity fluctuation profiles. These results are compared to those obtained from two DNS databases, including those of Vreman and Kuerten (2014) and (Moser et al., 1999). The agreement in both cases is excellent, and provides confidence in the single-phase flow field, within which we inject the particles.

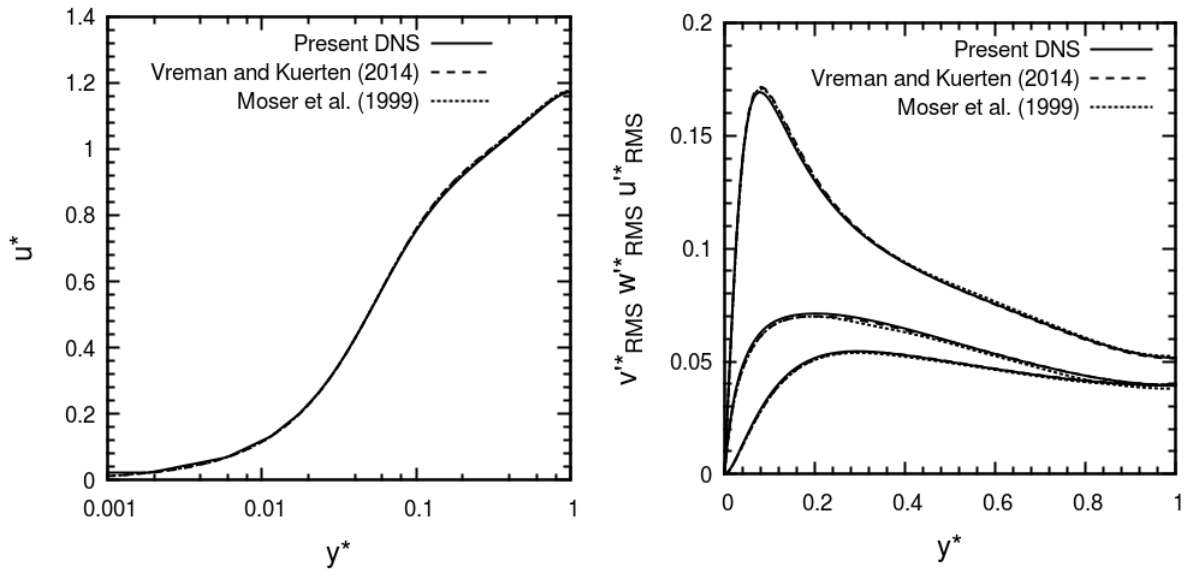


Figure 4: Statistical moments of unladen $Re_\tau = 180$ turbulent channel flow velocity field. Left: Mean streamwise velocity; Right: root-mean-square of streamwise, spanwise and wall-normal velocity fluctuations (top to bottom). Present work is compared with results of Vreman and Kuerten (2014) and Moser et al. (1999).

B. Particle-laden flow statistics

Five fully-coupled particle-laden turbulent flow simulations were performed in order to both demonstrate the performance of the agglomeration mechanism, and to elucidate the effect of particle diameter on collision and agglomeration behaviour. To determine these effects, it is important to isolate those which occur as a result of an increased volume fraction due to larger particles. As such, we consider two analysis regimes, one at fixed volume fraction and one at fixed particle number. In each case, we consider three different particle diameters of relevance to nuclear waste slurry flows, $d_p = 202.5 \mu m$, $286.4 \mu m$ and $405.0 \mu m$. Hence, particle numbers were chosen to match relevant key volume fractions, with a baseline case at $\phi_p = 10^{-3}$,

the solid volume fraction at which the first- and second-order flow statistics become significantly altered upon inclusion of interparticle collisions. The chemical and physical properties are chosen to match those of spherical calcite particles in water, with all properties presented in Table 2 (Tomas, 2007; Anh Ho and Sommerfeld, 2002). Particles are initially mono-dispersed and are injected randomly throughout the channel, ensuring no initial overlap. All coupling and agglomeration mechanisms were enabled from the first timestep after injection, and the particle-laden simulations were performed for 20,000 timesteps, corresponding to $t^* = 100$ in bulk time units, which is over 1000 times greater than the largest bulk particle relaxation timescale considered here. Fluid statistics were resampled during this period in order to determine the extent of two-way coupling effects on the continuous phase turbulence field. Figure 5 illustrates the momentum-coupling effects on the mean streamwise velocity profile for both analysis regimes. In both cases, there are only minimal differences which appear only in the region $y^* > 0.1$, wherein the mean streamwise velocity is reduced slightly. This effect is most evident for the fixed particle number simulation at $St^+ = 2$, which has the greatest volume fraction of particles out of all the sets considered here. This is as expected, and the magnitude scaling of this streamwise velocity reduction with Stokes number and volume fraction is widely documented for low Stokes numbers ($St^+ < 5$) (Zhao et al., 2015).

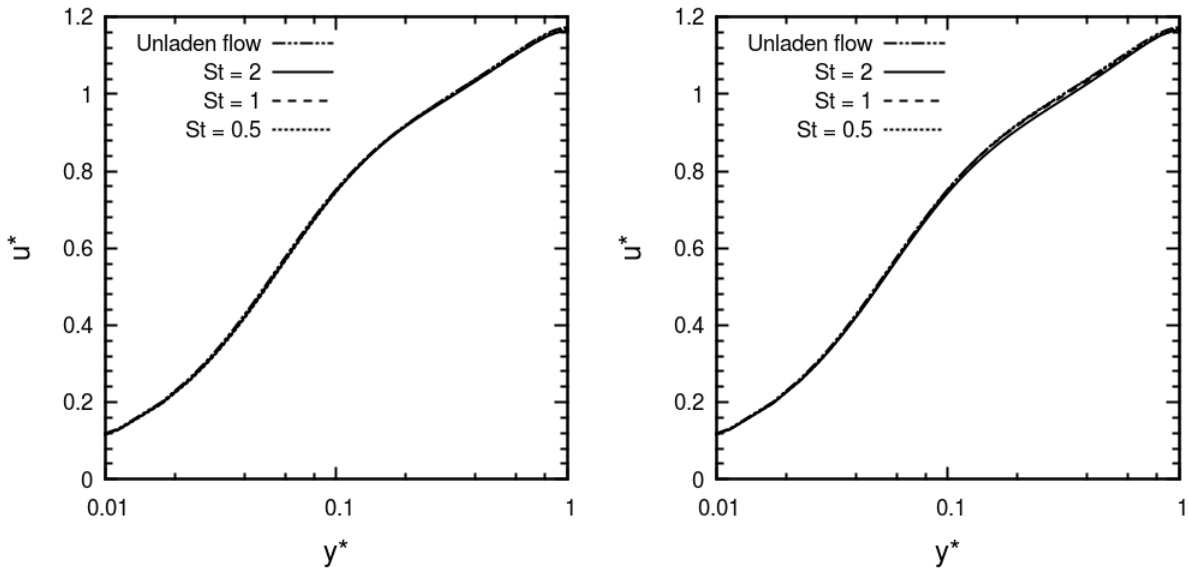


Figure 5: Effect of Stokes number on fluid mean streamwise velocity of $Re_\tau = 180$ turbulent channel flow. Left: Fixed volume fraction; Right: Fixed particle number.

The momentum coupling effects on the root-mean-square velocity fluctuations are illustrated in Figure 6. In all cases, the particles act to slightly dampen the turbulence intensities, again only very marginally. The greatest effect is also observed for the fixed particle number simulation at $St^+ = 2$, which dampens the peak streamwise turbulence intensity at $y^* = 0.08$, as well as at the centre of the channel. The other two components are also reduced slightly in the outer layer. Clearly, due to the

low particle-fluid density ratio inherent in liquid-solid flows, particle-fluid momentum feedback is low, and as such, its effects are only minimal and could be ignored. Future work on such flows could therefore consider neglecting this mechanism in the calculations to reduce compute-time, however we chose to include such coupling to demonstrate the lack of effect and for completeness in terms of the accuracy of the results.

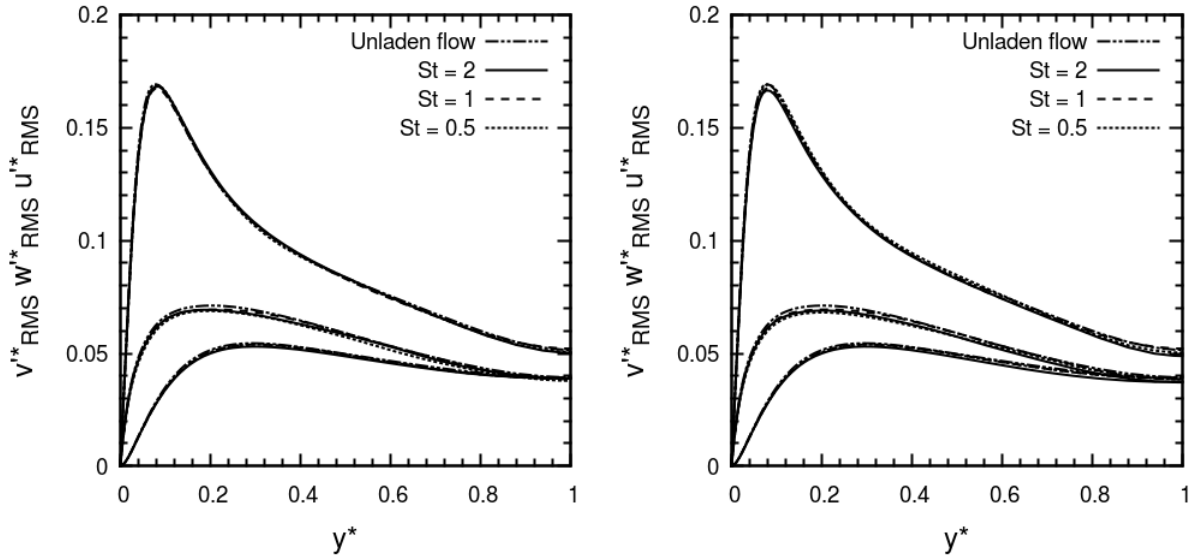


Figure 6: Effect of Stokes number on fluid root-mean-square of streamwise, spanwise and wall-normal velocity fluctuations (top to bottom) of $Re_\tau = 180$ turbulent channel flow. Left: Fixed volume fraction; Right: Fixed particle number.

Particle velocity statistics were sampled throughout the entire channel over the course of the particle-laden simulations. Since the agglomerating system is temporally dynamic such that the mean particle diameter (and Stokes number) is changing with time, the statistics presented here are obtained from taking averages over the entire particle-laden simulations, unless otherwise stated.

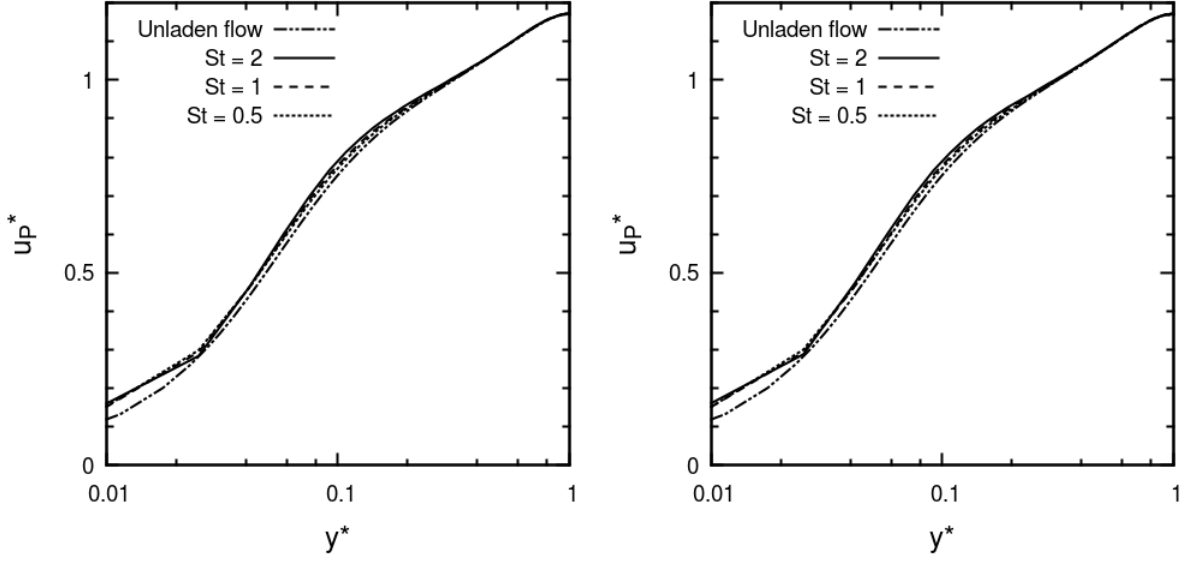


Figure 7: Effect of Stokes number on mean streamwise velocity of particulate phase of $Re_\tau = 180$ turbulent channel flow. Left: Fixed volume fraction; Right: Fixed particle number.

Figure 7 presents the mean streamwise particle velocity profiles for all cases. Due to a lack of validation data or alternative predictions for the particle properties employed, we do not include here any validation for the particulate phase results, however an alternative validation can be found in Mortimer et al. (2019) which utilizes the same LPT solver. As expected, the particles exhibit very similar macroscopic behaviour to that of the fluid phase, since their Stokes numbers are low and they have little or no difficulty adjusting to the local fluid velocity. The most notable difference is that the $St^+ = 2$ particles exhibit behaviour in the $0.02 \leq y^* \leq 0.4$ region where they travel faster than the fluid. In Figure 8, we consider the root-mean-square velocity fluctuations for the particles alongside those of the fluid. In terms of these results, both the fixed volume fraction and fixed particle number regimes exhibit very similar behaviour, indicating a lack of particle number dependency on velocity deviations. As the Stokes number is increased, the turbulence intensities are enhanced compared to those of the fluid phase, with the greatest enhancements occurring in the buffer region for the streamwise component, and the bulk flow for the other two components. These observations are agreement with expectations and previous studies (Zhao et al., 2015; Kulick et al., 1994) in which it was shown that increased slip velocities due to increasing particle inertia decorrelate the particle motion from the local flow field.

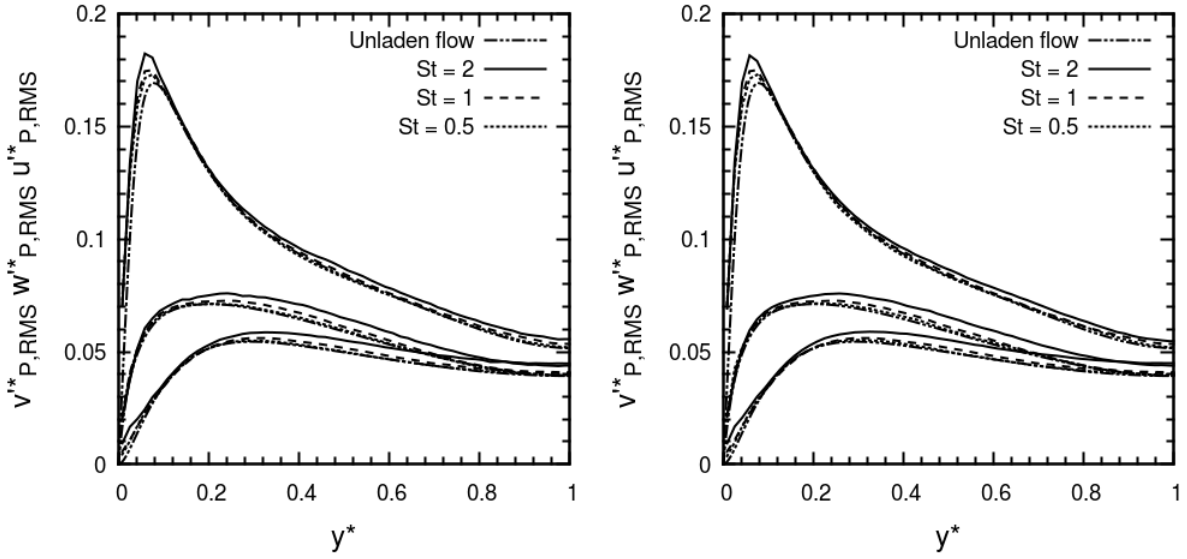


Figure 8: Effect of Stokes number on root-mean-square of streamwise, spanwise and wall-normal velocity fluctuations (top to bottom) of particulate phase of $Re_\tau = 180$ turbulent channel flow. Left: Fixed volume fraction; Right: Fixed particle number.

Figure 9 shows the effect of particle diameter on the concentration of particles relative to the initial concentration throughout the channel flow domain. It should be noted here that the mean value in these distributions is not unity, since the total number of particles decreases as the simulation is advanced. In the fixed volume fraction case, particle concentration peaks both at the centre of the channel and at the wall for the largest particles. It is clear that both the $St^+ = 1$ and $St^+ = 2$ particles exhibit preferential concentration very close to the wall, undergoing turbophoresis which causes them to congregate in regions of low turbulence kinetic energy. This is not true of the most tracer-like particles ($St^+ = 0.5$) which exhibit no preferential accumulation in the wall region over the time considered. It should be noted here that later samples of concentration do indicate a very slow migration towards the wall for the low Stokes number particles, as observed in previous work (Marchioli and Soldati, 2002). Moving to the bulk flow, particle concentration is shown to be determined by particle size, with larger particles exhibiting lower concentrations.

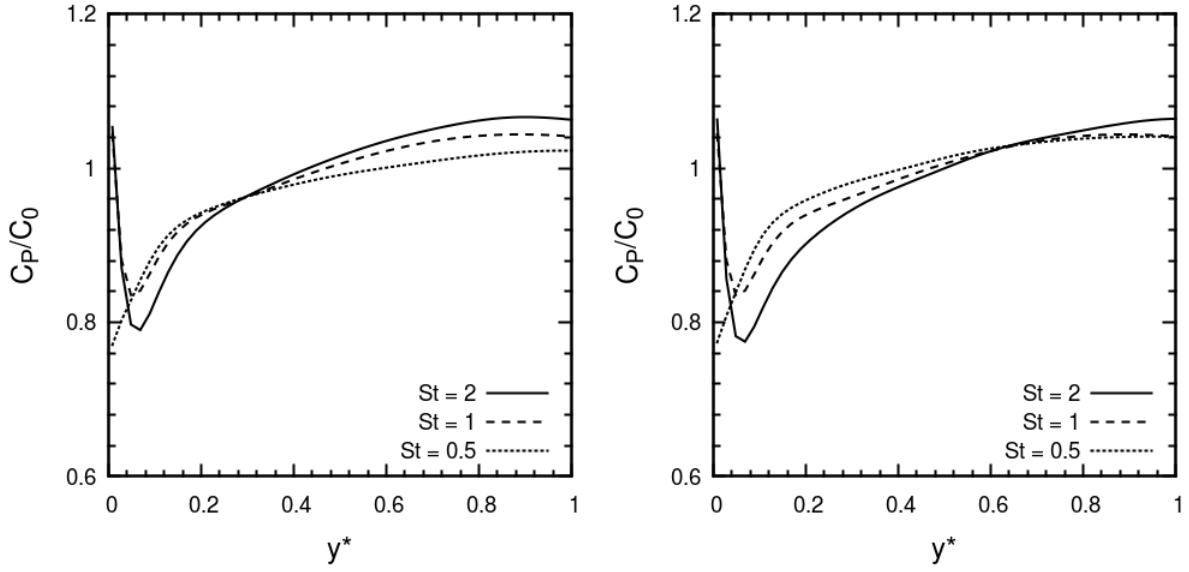


Figure 9: Effect of Stokes number on mean particle concentration relative to initial concentration across wall-normal direction of the channel. Sample time is $50 \leq t^* \leq 100$. Left: Fixed volume fraction; Right: Fixed particle number.

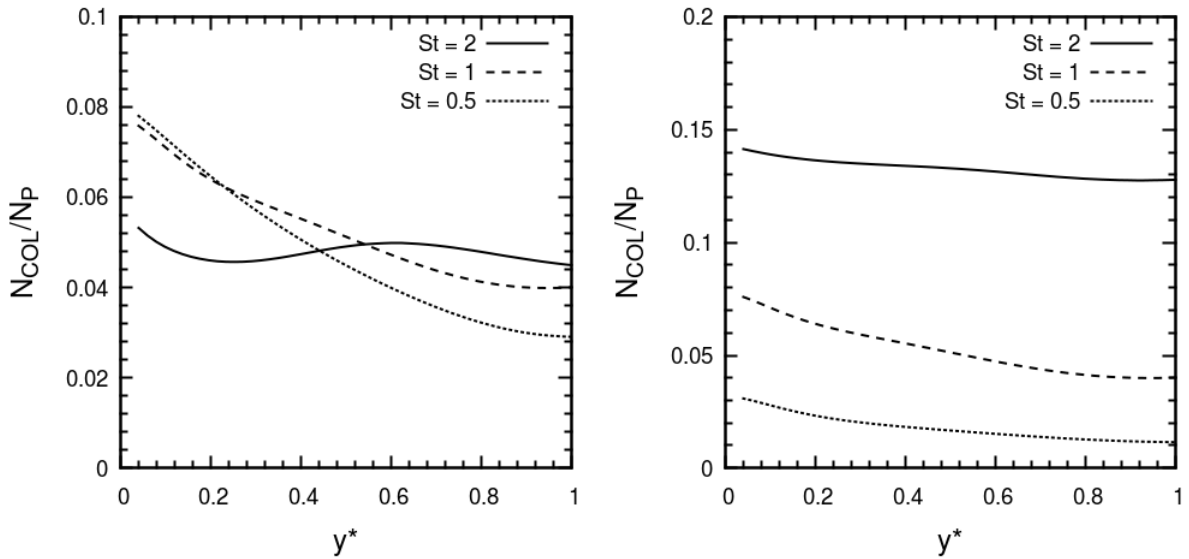


Figure 10: Effect of Stokes number on mean particle collision rate normalized by initial number of injected primary particles across wall-normal direction of the channel. Sample time is $50 \leq t^* \leq 100$. Left: Fixed volume fraction; Right: Fixed particle number.

The point at which the three concentration profiles coincide (and any trends reverse) greatly depends on whether the particle number or volume fraction is varied, with the former occurring at $y^* = 0.3$ and the latter occurring at $y^* = 0.6$. This is likely due to the increased agglomeration rate in the outer layer of the channel for larger particles, lowering the concentration in the bulk region, which is discussed further below.

Figure 10 shows the collision rate normalized by the initial particle number for both regimes considered. In the fixed volume fraction case the collision rates are relatively similar, with smaller particles showing a preference for collision closer to the wall. This is an interesting result since the particle concentration is lowest in that region, however, the increased particle

turbulence intensities encourage particles to collide. Similar observations for collision rates were made by Yamamoto et al. (2001) with low Stokes number particles showing preferential collisions close to the wall and larger particles exhibiting a more homogeneous profile. The dip for $St^+ = 2$ particles around $y^* = 0.2$ is due to the interplay between the collision rate lowering effect of low local concentration (comparing with Figure 9) and the increased velocity fluctuation effect close to the wall. For the fixed particle number regime, all three profiles are similar, such that the collision rate is greatest close to the wall and, as expected, the largest particles collide more frequently. These observations are also in line with previous simulations (Li et al., 2001), wherein collision rates were found to be greatest in the wall region and to scale inversely with particle diameter for a fixed volume fraction.

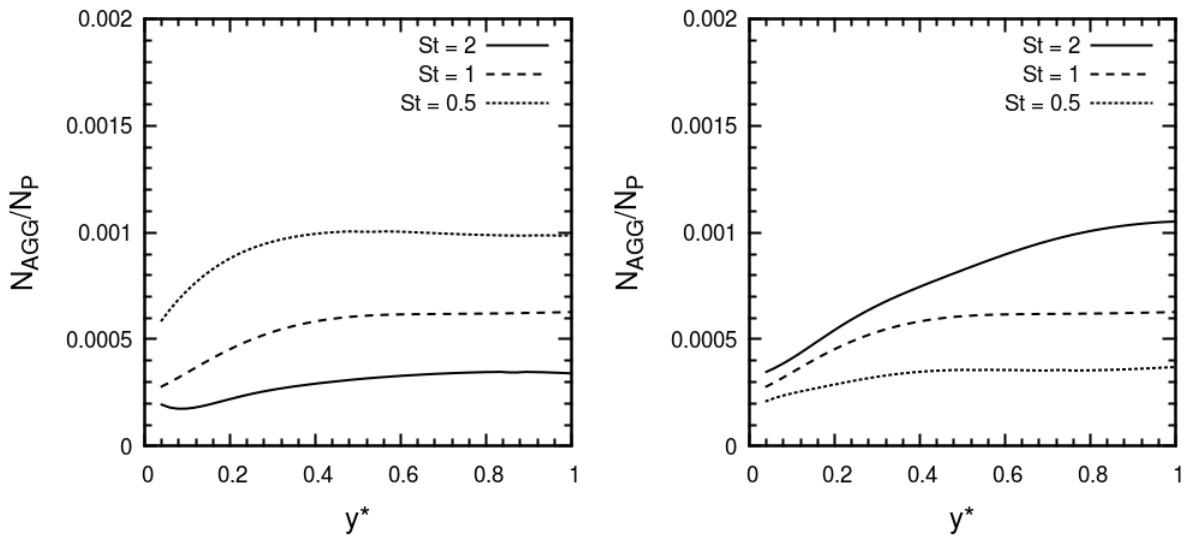


Figure 11: Effect of Stokes number on mean number of agglomeration events per timestep normalized by initial number of injected primary particles across wall-normal direction of the channel. Sample time is $50 \leq t^* \leq 100$. Left: Fixed volume fraction; Right: Fixed particle number.

The mean number of agglomeration events per timestep across the channel is plotted in Figure 11. For the fixed volume fraction simulations, the number of agglomerations is approximately constant in the bulk and falls off in the wall region, with smaller particles showing greater agglomeration numbers. The diameter (or Stokes number) dependency is expected here, since the number of particles is increased as the Stokes number is lowered to preserve the volume fraction. What is not expected is the relationship between agglomeration events and collision rates, as more agglomerations are observed in the regions which exhibit the fewest collisions. This implies, for the parameters studied, that agglomeration is more likely to be driven by locally favourable dynamics rather than regions of increased collisions. The fixed particle number simulations also indicate that agglomeration events are favoured in the bulk region of the flow for all three particle diameters, however, in this case, since the number of collisions for larger particles is increased, the $St^+ = 2$ particles exhibit the greatest number of normalized

collisions. The general decrease of agglomeration frequency with Stokes number at constant volume fraction is also in accordance with the findings of Njobuenwu and Fairweather (2017) who obtained similar results using LES, however only bulk interaction properties were detailed, and we observe that this trend continues to hold for $St^+ > 1$.

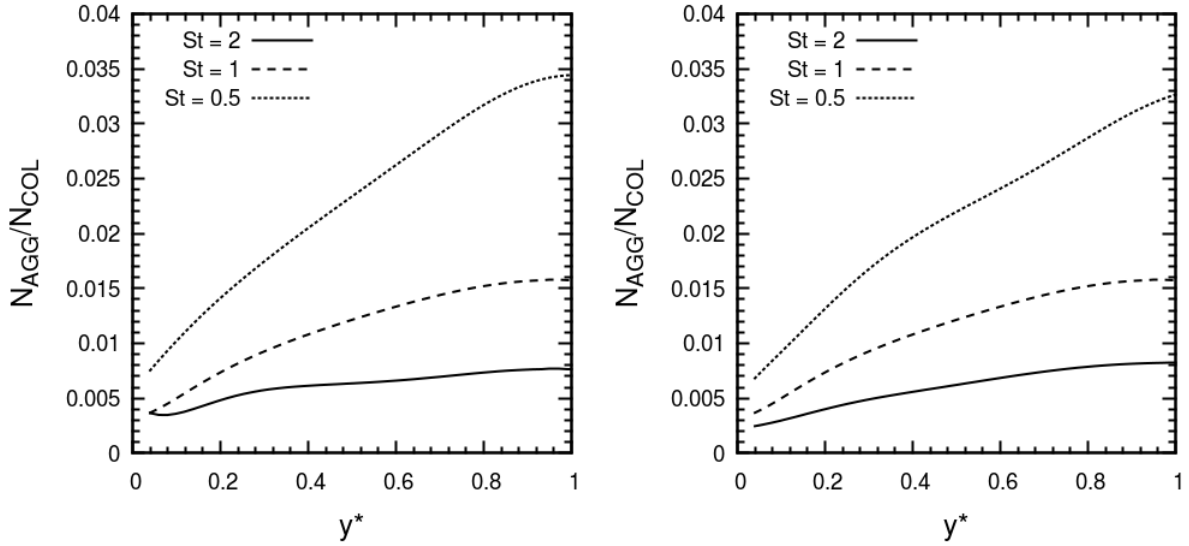


Figure 12: Effect of Stokes number on mean particle agglomeration rate across wall-normal direction of the channel. Sample time is $50 \leq t^* \leq 100$. Left: Fixed volume fraction; Right: Fixed particle number.

Figure 12 illustrates the mean agglomeration rate (N_{AGG}/N_{COL}), sometimes referred to as an agglomeration efficiency, across the channel domain. To clarify, this quantity is the mean probability of agglomeration given that a collision has occurred in this statistical region. The fixed volume fraction and fixed particle number plots are very similar, demonstrating that the post-collision particle agglomeration dynamics are independent of particle number, which is reasonable as particle number drives mostly the collision density and not the outcome. Here we observe that: a) collisions which occur in the centre of the channel have a greater chance of resulting in an agglomeration event, and b) the magnitude of this effect scales inversely with the Stokes number or, in particular, the particle diameter.

It can be determined that a greater agglomeration efficiency in the centre of the channel implies that the bulk region of the flow has more favourable conditions for agglomeration, meaning that the left hand side of Eqn. (7) is sufficiently small in the bulk flow region. The associated implication is that particle collisions taking place in the bulk flow region (which has a lower Reynolds number based on the Taylor microscale) are less impactful, such that $\mathbf{u}_{p,r}^*$ is small. This is likely to be the case since the particle root-mean-square velocity fluctuations are lowest in this region, and hence two randomly colliding particles are likely to have similar velocities. This is confirmed in Figure 13, which gives results for the magnitude of the relative particle collision velocity throughout the channel. As expected, particles colliding in the bulk region of the channel flow possess much lower relative velocities than those close to the wall, encouraging agglomeration. Furthermore, in the wall region this magnitude

is greatly dependent on particle diameter, with larger particles colliding with increased relative velocities. Both analysis regimes demonstrate identical behaviour in terms of their Stokes number dependence.

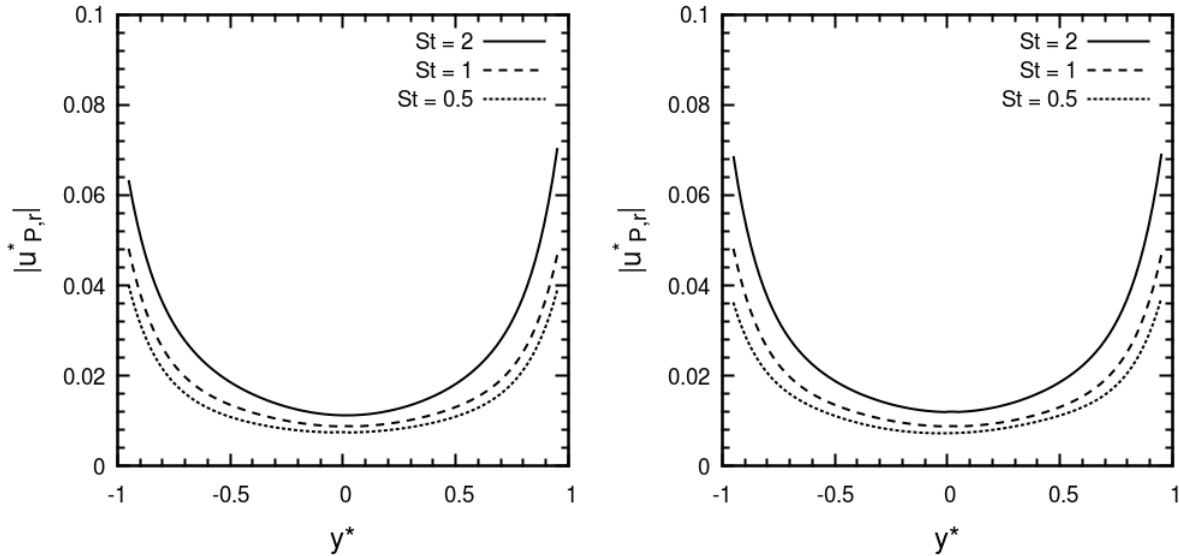


Figure 13: Effect of Stokes number on mean relative particle collision velocity across wall-normal direction of the channel. Sample time is $50 \leq t^* \leq 100$. Left: Fixed volume fraction; Right: Fixed particle number.

Figure 14 illustrates the mean collision angle calculated using $\theta_{COL} = \cos^{-1}(\mathbf{u}_1^* \cdot \mathbf{u}_2^* / (|\mathbf{u}_1^*| |\mathbf{u}_2^*|))$ which helps determine the way in which the particles collide. For instance, low angles indicate both particles are travelling in the same direction when the collision occurs, likely tracing the same flow streamline. Again, the bulk flow demonstrates a regime in which the particles collide with very small angles (below one degree), which increases greatly in the wall region. We also observe that as the particle diameter increases, the mean angle at which a collision occurs also increases in all regions of the channel flow. Whether volume fraction or particle number is varied has little effect on the resulting collision dynamics.

We can determine from the results given in the previous two figures that the agglomeration mechanism is highly dependent on the local turbulence properties, which drive the manner in which particles collide in a given region of the channel flow. Although collisions are favoured in the wall region due to the high root-mean-square velocity fluctuations of both the fluid and particle phases, the dominant influence on particle agglomeration is favourable local flow conditions, such that particles collide with low relative velocities.

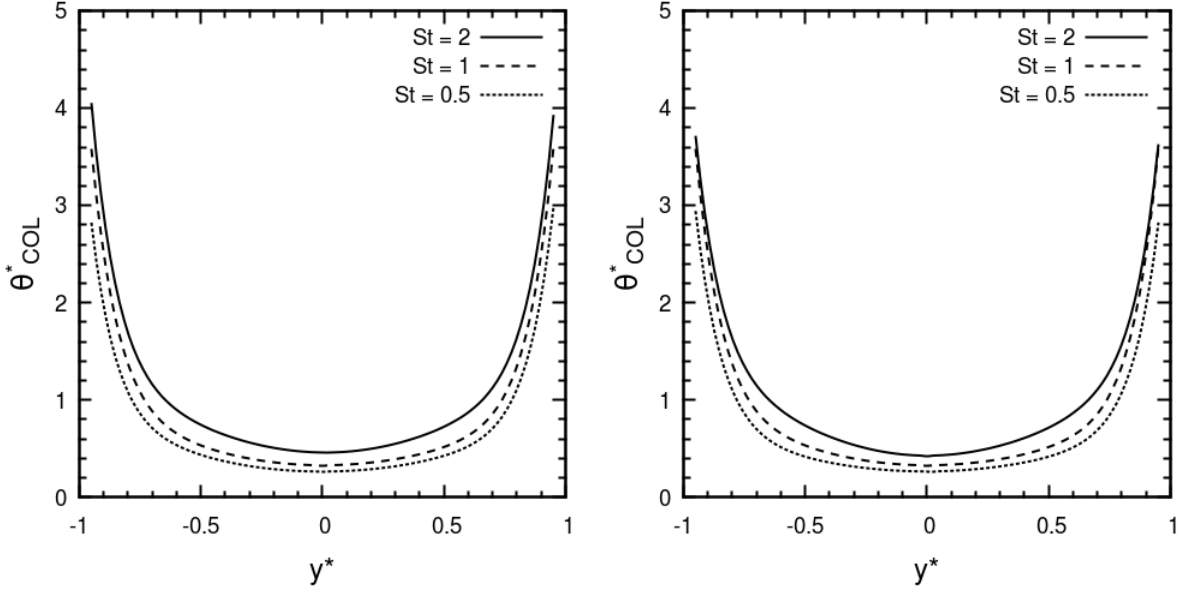


Figure 14: Effect of Stokes number on mean particle collision angle across wall-normal direction of the channel. Sample time is $50 \leq t^* \leq 100$. Left: Fixed volume fraction; Right: Fixed particle number.

The latter observation, that the agglomeration efficiency increases with the Stokes number, is explained by the right hand side of Eqn. (8) which is inversely proportional to d_p^* and, as such, the particles need to do more work to evade agglomeration if they are smaller, hence their collision is more likely to result in an agglomeration event, given a collision. Larger particles were also shown to collide with greater relative particle velocities, or kinetic energies, and so the left hand side of Eqn. (8) is more likely to be dominant. This implies that as the particles begin to form agglomerates, the mean overall agglomeration rate should slowly decrease, since the mean particle diameter will be increased. The diameter dependence observation agrees with previous predictions (Anh Ho and Sommerfeld, 2002), however these were performed in isotropic turbulence and so the dispersive property-related findings were missed.

C. Temporal evolution of collision and agglomeration events

In this subsection, in order to help predict the stability and dynamics of agglomerating multi-phase flows at long timeframes, we shall consider the time-evolution of various quantities relating to concentration, collisions and agglomeration. Firstly, Figure 15 illustrates the total number of collision events over $0 \leq t^* \leq 50$. Clearly, the mean collision rate is constant and stable for all simulations considered. The same diameter dependency as exhibited in Figure 10 is also demonstrated for both regimes. Similar observations can be made for the number of agglomeration events in Figure 16, with the number of events per timestep constant over the timeframe considered.

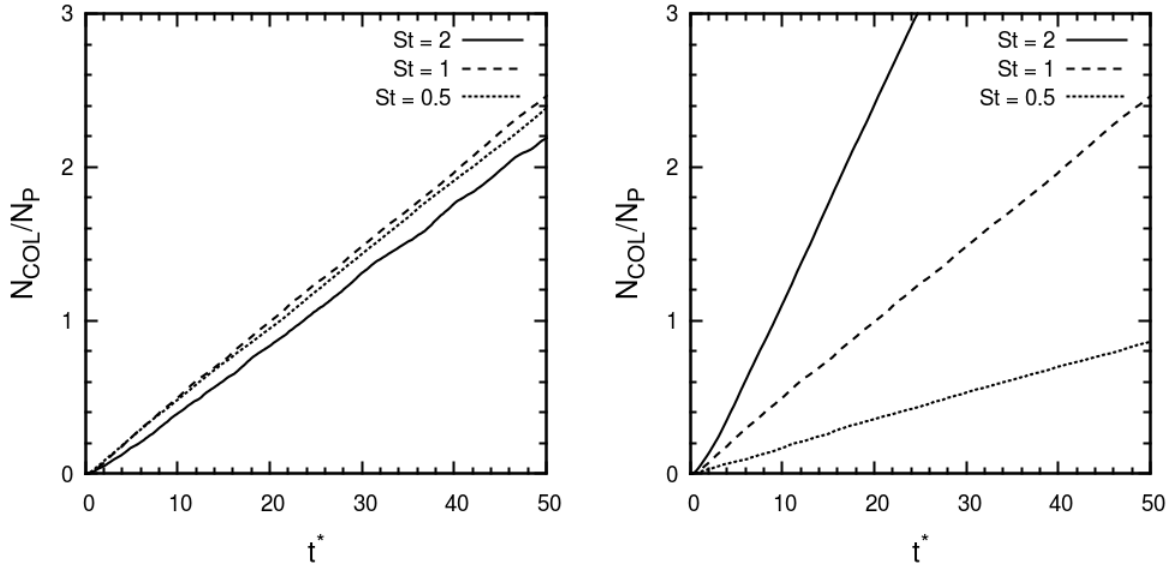


Figure 15: Effect of Stokes number on temporal evolution of total number of particle-particle collision events normalized by the initial number of injected primary particles. Left: Fixed volume fraction; Right: Fixed particle number.

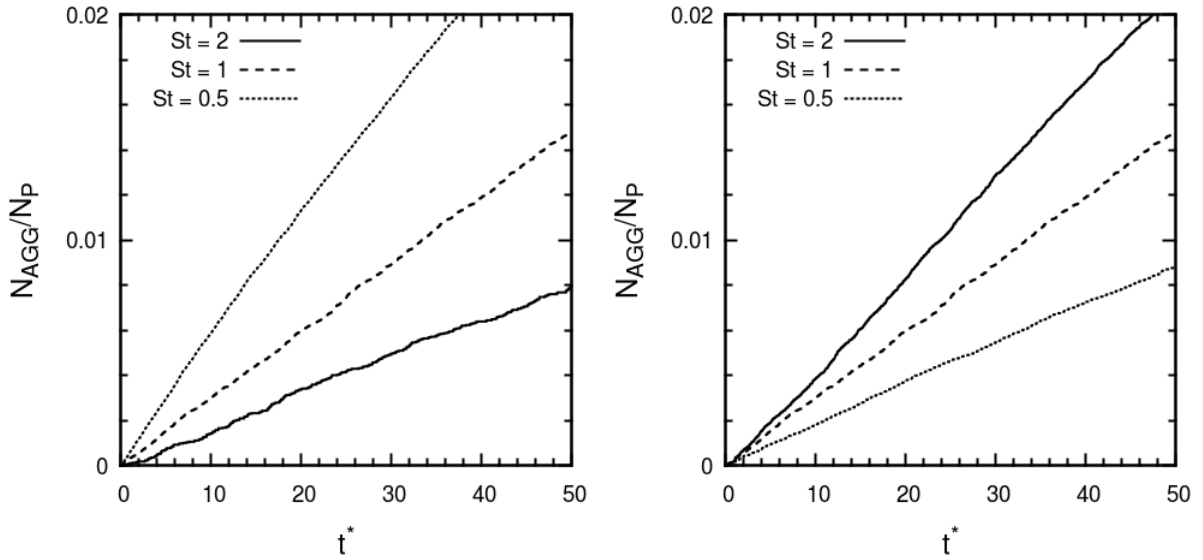


Figure 16: Effect of Stokes number on temporal evolution of total number of particle-particle agglomeration events normalized by the initial number of injected primary particles. Left: Fixed volume fraction; Right: Fixed particle number.

Figure 17 demonstrates a steady agglomeration rate after around $t^* = 10$ with minor statistical fluctuations before then. In agreement with Figure 12, both the fixed volume fraction and fixed particle number regimes exhibit the same agglomeration rate for a specific particle diameter once the system has settled. A very minor downwards gradient is expected here, since as the system starts to agglomerate, there are fewer (and larger) particles left to interact.

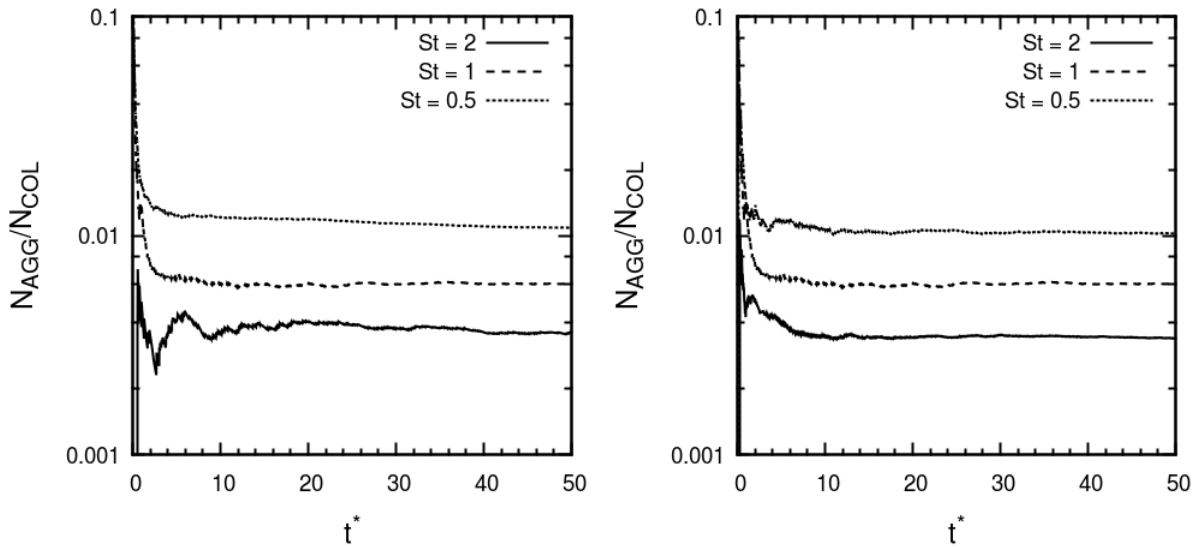


Figure 17: Effect of Stokes number on temporal evolution of the agglomeration rate normalized by the initial number of injected primary particles. Left: Fixed volume fraction; Right: Fixed particle number.

Naturally, over very long timescales, the system will reach a state in which either: a) all particles have agglomerated to form one large particle, or b) the particles are all large enough such that Eqn. (8) will never be satisfied and, as such, particles will no longer agglomerate. The latter option is the most realistic, and other studies (Njobuenwu and Fairweather, 2018) have also considered the effect of break-up which also creates a limiting factor for the particle size distribution.

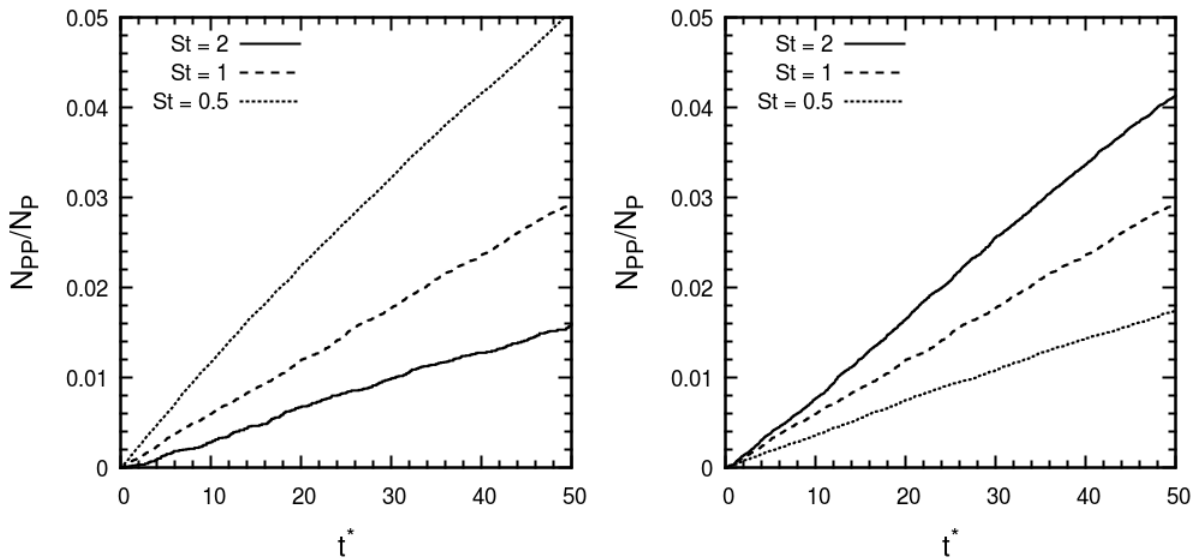


Figure 18: Effect of Stokes number on temporal evolution of mean number of agglomerated primary particles normalized by the initial number of injected primary particles. Left: Fixed volume fraction; Right: Fixed particle number.

Figure 18 and Figure 19 demonstrate the time evolution of the number of agglomerated primary particles and the total proportion of particle agglomerates (of any size). These quantities all increase at a constant rate, in line with the number of agglomeration events.

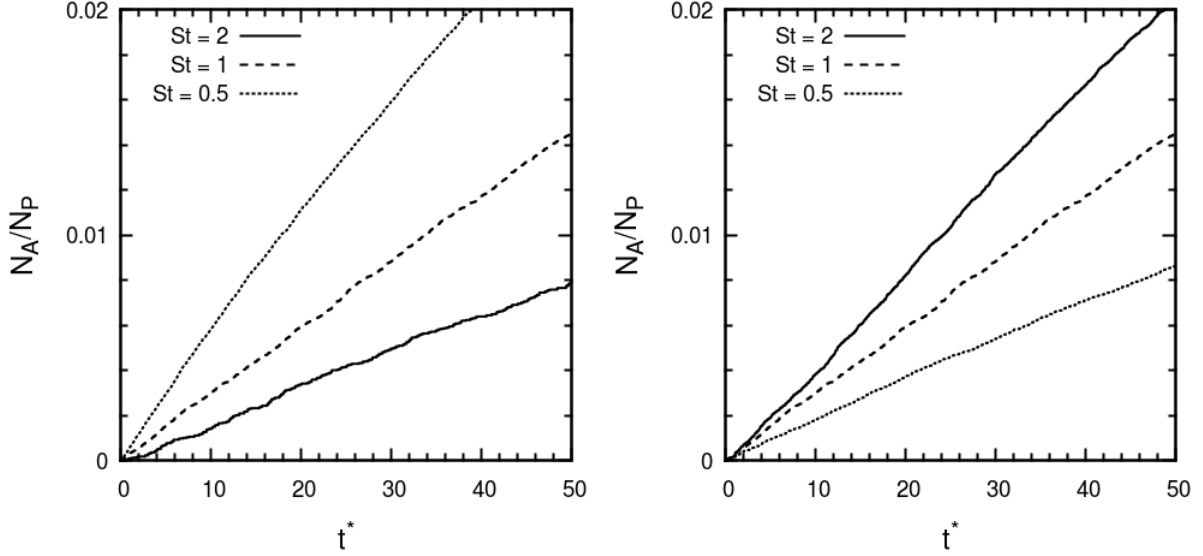


Figure 19: Effect of Stokes number on temporal evolution of mean number of total particle agglomerates (of any size) normalized by the initial number of injected primary particles. Left: Fixed volume fraction; Right: Fixed particle number.

Finally, Figure 20 demonstrates the time evolution of agglomerates of a certain particle number ranging from primary particles ($N = 1$) to quadruplets ($N = 4$). For all cases considered, the agglomeration rate over the course of each simulation is approximately constant. For the fixed volume fraction simulations, almost 10% of the low Stokes number particles undergo agglomeration and become part of higher-order aggregates, with over 0.01% of the original injected particles forming $N = 4$ type agglomerates. As the Stokes number is increased, the agglomeration rate is reduced and the time at which higher-order aggregates are formed is extended. In the fixed particle number simulations, as observed earlier, the largest particles undergo agglomeration more quickly than the smaller particles, since the collision rate in the favourable bulk flow region is high. Interestingly, triplet type agglomerates are formed at approximately the same rate for the two larger particle sizes, which is due to the condition that the Stokes number of a particle increases proportionally to its current Stokes number as the order of the agglomerate increases, and so the collision behaviour of the two sizes of particle becomes more comparable.

The temporally evolving results exhibit slower particle aggregation than those predicted in similar studies (Njobuenwu and Fairweather, 2017), however these employed an LES technique, which has been shown to underpredict turbophoretic effects (Kuerten and Vreman, 2005), meaning that particles spend more time in the agglomeration preferred regions.

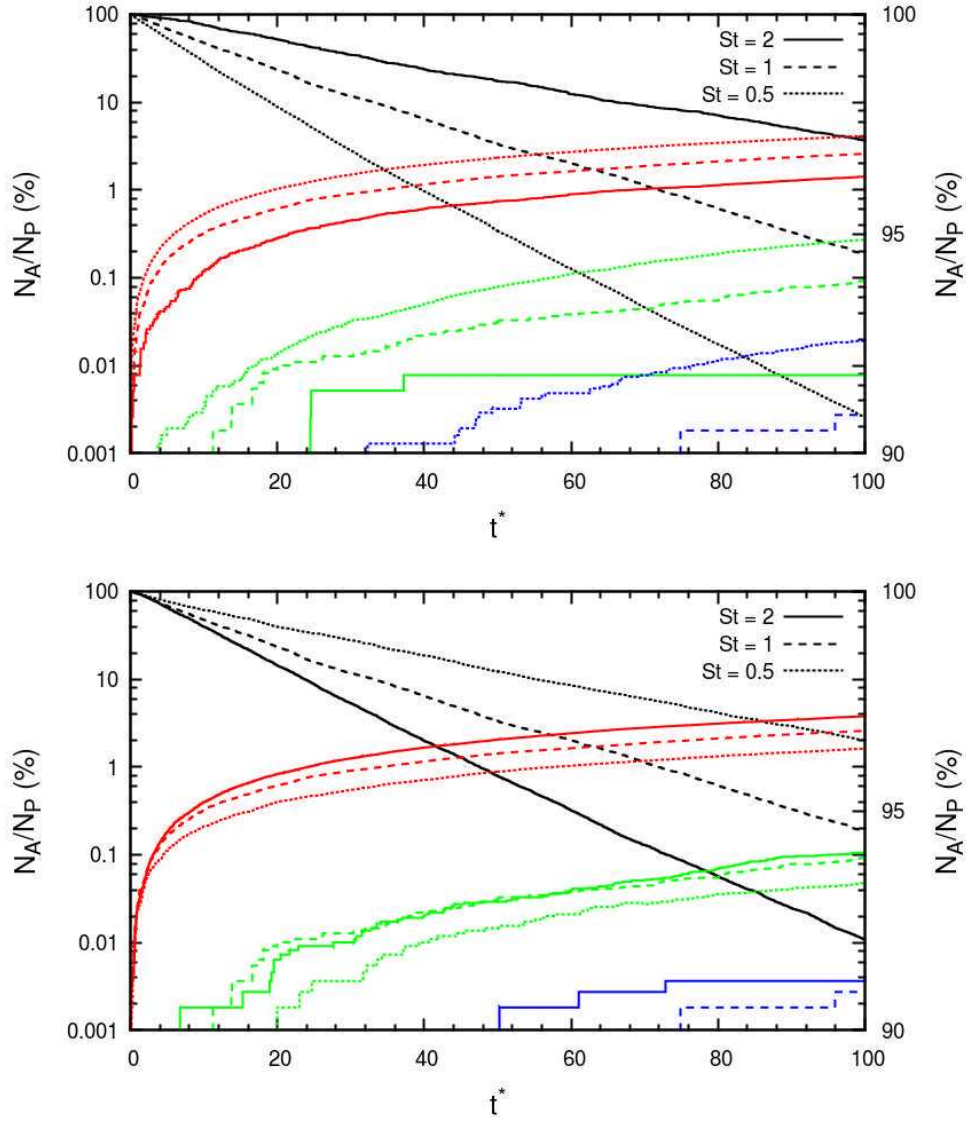


Figure 20: Effect of Stokes number on temporal evolution of the number of agglomerates of size N . Right hand scale, Black: $N=1$; and left hand scale, red: $N=2$; green: $N=3$; blue: $N=4$. Upper: Fixed volume fraction; Lower: Fixed particle number.

IV. CONCLUSIONS AND OUTLOOK

Knowledge surrounding the formation of agglomerate structures in solid particulate transport flows is sparse within the literature, with very few computational studies using high fidelity methods to investigate such phenomena. In this work, direct numerical simulation and Lagrangian particle tracking techniques have been used to investigate agglomerating particle-laden liquid-solid flows in order to improve our understanding of the small-scale aggregation mechanisms involved in such systems. To improve upon previous work, DNS has been employed to fully resolve the local particle-scale turbulence fields and obtain a more in-depth, accurate representation of trajectories which result in collision and agglomeration events. The LPT has also been developed for high accuracy, solving for all relevant terms of the Maxey-Riley equation as well as being two- and four-

way coupled with the flow field, with the latter based on the hard-sphere approach. A deterministic energy-based agglomeration algorithm has been implemented and demonstrated to produce reliable results for flows with chemical and physical properties matching those of simulants used in the design of nuclear waste processing systems. All of these features are critical in modelling such systems since their hydrodynamic and electrochemical interactions operate at a multitude of scales, which in turn necessitates a highly resolved single-phase flow solution as obtained in the present work. The geometry used here is that of a channel flow, and the continuous phase represents a pressure-drop driven flow at a shear Reynolds number, $Re_\tau = 180$. The present analysis considered variations of particle diameter, d_p^* , and its effect on the dispersion, collision and agglomeration behaviour of calcite particles in water. Volume fractions were chosen to ensure all flows take place in the regime where particle collisions dynamics are dominant in order to promote subsequent agglomeration.

In terms of momentum-coupling, effects due to particle forcing on the fluid were minimal, with only a very slight reduction observed in the bulk flow region mean streamwise velocity and spanwise turbulence intensity, an effect scaling with the Stokes number. The particle first- and second-order statistics resembled those of the fluid, with some minor deviations where they travel faster than the fluid in the wall region. Furthermore, as particle diameter was increased, the root-mean-square of the velocity fluctuations was enhanced compared to those of the fluid, an effect caused by increased slip velocities for larger particles. In both fixed volume fraction and fixed particle number cases, the particles with the two largest diameters exhibited preferential concentration close to the wall, whereas the tracer-like particles congregated in the bulk flow region. At fixed particle number, the increased aggregation exhibited by the larger particles meant that the particle concentration in the bulk flow region was lower than that exhibited at fixed volume fraction.

Collision rates at fixed volume fraction were similar for all three particle diameters, with the larger particles showing a preference for collision at the centre of the channel, and smaller particles showing a preference for the wall. In contrast, at fixed particle number, collision rates scaled directly with the Stokes number in all regions of the channel. The number of agglomeration events in the fixed volume fraction simulations was stable in the bulk flow region, with a drop off towards the wall region, whereas for fixed particle number, agglomerations were increased at the centre of the channel, particularly so for the particles with the largest diameter. Comparing this to the number of collisions in that region, which was at a minimum, it is concluded that the increased agglomeration events for larger particles is due to favourable local dynamics. This is further confirmed by considering the agglomeration rate given a collision has already occurred, which is almost identical for the fixed volume fraction and fixed particle number simulations. From this we conclude there exists a clear preference for particle agglomeration to occur in the centre of the channel, with smaller particles exhibiting a greater agglomeration efficiency. By considering the agglomeration condition, it is suggested that the reason agglomeration is favoured in this region is because the

particle root-mean-square velocity fluctuations are low and hence colliding particles are likely to have low relative velocities at the moment of collision. This is confirmed through collision event analysis, with the collisions in the bulk flow possessing much lower relative particle velocities and collision angles. Agglomeration suppression at increased Stokes numbers (or specifically particle diameters) was also observed for fixed volume fraction simulations, an effect previously noted in work which varied the particle density, for particles with increased mass (Anh Ho and Sommerfeld, 2002).

Comparing agglomeration frequency, particles with larger diameter agglomerated more slowly in the fixed volume fraction simulations than in the fixed particle number case. This is likely due to the number of collisions scaling with particle number, which increases proportional to N_p^2 . The temporal evolution of agglomeration rates was very similar for both fixed volume fraction and fixed particle number cases, with smaller primary particles exhibiting a greater tendency to agglomerate, given a collision had already occurred. Lastly, the distribution of primary particles, agglomerates of any size, and agglomerates of specific sizes have been compared over the course of each simulation. All the systems considered undergo substantial agglomeration, with primary particle percentages decreasing by almost 10% in some cases. This has consequences for long-time predictions of such flows, as the mean diameter of the particles, and hence Stokes number, will increase over time and therefore standard LPT simulations (even those four-way coupled) will deviate from reality since Stokes-based dynamics will lead to inaccurate predictions. While this work has considered liquid-solid flows, the study of gas-solid flows will enable the consideration of higher Stokes numbers, $St^+ = O(10)$, where mechanisms such as low speed streak particle accumulation are likely to play a further important role in preferential collision and subsequent agglomeration events. Lastly, in order to further validate the observations made, experiments should be performed to compare temporally evolving particle size distributions in similar agglomerating flows, which will involve performing simulations with gravity and buoyancy forces included in the LPT force-balance equation. Upon doing so, the present work will aid in determining any new dispersion, collision or agglomeration effects as gravity-induced rather than due solely to interaction with the turbulence field.

V. ACKNOWLEDGEMENTS

The authors are grateful for funding from the UK Engineering and Physical Sciences Research Council through the TRANSCEND (Transformative Science and Engineering for Nuclear Decommissioning) project (EP/S01019X/1).

VI. REFERENCES

- M. Alletto. "Numerical investigation of the influence of particle-particle and particle-wall collisions in turbulent wall-bounded flows at high mass loadings." PhD thesis, Helmut-Schmidt University, 2014,
- N. Almohammed and M. Breuer. "Modeling and simulation of agglomeration in turbulent particle-laden flows: A comparison between energy-based and momentum-based agglomeration models." *Powder Technology*. **294**, 373-402. (2016).

- C. Anh Ho and M. Sommerfeld. "Modelling of micro-particle agglomeration in turbulent flows." *Chemical Engineering Science*. **57**, 3073-3084. (2002).
- B. Balakin, A. C. Hoffmann and P. Kosinski. "The collision efficiency in a shear flow." *Chemical Engineering Science*. **68**, 305-312. (2012).
- M. Boivin, O. Simonin and K. D. Squires. "Direct numerical simulation of turbulence modulation by particles in isotropic turbulence." *Journal of Fluid Mechanics*. **375**, 235-263. (1998).
- M. Breuer and N. Almohammed. "Modeling and simulation of particle agglomeration in turbulent flows using a hard-sphere model with deterministic collision detection and enhanced structure models." *International Journal of Multiphase Flow*. **73**, 171-206. (2015).
- G. Charalampous and Y. Hardalupas. "Collisions of droplets on spherical particles." *Physics of Fluids*. **29**, 103305. (2017).
- M. Chen, K. Kontomaris and J. McLaughlin. "Direct numerical simulation of droplet collisions in a turbulent channel flow. Part I: collision algorithm." *International Journal of Multiphase Flow*. **24**, 1079-1103. (1999).
- R. Chen, L. Zhang, D. Zang and W. Shen. "Blood drop patterns: Formation and applications." *Advances in Colloid and Interface Science*. **231**, 1-14. (2016).
- Y. J. Choi and N. Djilali. "Direct numerical simulations of agglomeration of circular colloidal particles in two-dimensional shear flow." *Physics of Fluids*. **28**, 013304. (2016).
- J. Chun, T. Oh, M. Luna and M. Schweiger. "Effect of particle size distribution on slurry rheology: Nuclear waste simulant slurries." *Colloids and Surfaces A: Physicochemical and Engineering Aspects*. **384**, 304-310. (2011).
- A. Daitche. "On the role of the history force for inertial particles in turbulence." *Journal of Fluid Mechanics*. **782**, 567-593. (2015).
- F. F. Dizaji and J. S. Marshall. "An accelerated stochastic vortex structure method for particle collision and agglomeration in homogeneous turbulence." *Physics of Fluids*. **28**, 113301. (2016).
- J. K. Eaton. "Two-way coupled turbulence simulations of gas-particle flows using point-particle tracking." *International Journal of Multiphase Flow*. **35**, 792-800. (2009).
- J. K. Eaton and J. Fessler. "Preferential concentration of particles by turbulence." *International Journal of Multiphase Flow*. **20**, 169-209. (1994).
- S. Elghobashi. "On predicting particle-laden turbulent flows." *Applied Scientific Research*. **52**, 309-329. (1994).
- S. Elghobashi and G. C. Truesdell. "Direct simulation of particle dispersion in a decaying isotropic turbulence." *Journal of Fluid Mechanics*. **242**, 655-700. (2006).
- M. Fairweather and J.-P. Hurn. "Validation of an anisotropic model of turbulent flows containing dispersed solid particles applied to gas–solid jets." *Computers & Chemical Engineering*. **32**, 590-599. (2008).
- J. R. Fessler, J. D. Kulick and J. K. Eaton. "Preferential concentration of heavy particles in a turbulent channel flow." *Physics of Fluids*. **6**, 3742-3749. (1994).
- P. F. Fischer, J. W. Lottes and S. G. Kerkemeier. 2008. *Nek5000*. [Online]. [Accessed 1st September]. Available from: <http://nek5000.mcs.anl.gov/>
- D. Folini, S. Uhl and P. Kaufmann. "Lagrangian particle dispersion modeling for the high Alpine site Jungfrauoch." *Journal of Geophysical Research: Atmospheres*. **113**, (2008).
- M. Fujita and Y. Yamaguchi. "Multiscale simulation method for self-organization of nanoparticles in dense suspension." *Journal of Computational Physics*. **223**, 108-120. (2007).
- D. Guha, P. A. Ramachandran and M. P. Dudukovic. "Flow field of suspended solids in a stirred tank reactor by Lagrangian tracking." *Chemical Engineering Science*. **62**, 6143-6154. (2007).

- C. Henry, J. Minier, J. Pozorski and G. Lefèvre. "A new stochastic approach for the simulation of agglomeration between colloidal particles." *Langmuir*. **29**, 13694-13707. (2013).
- H. Homann and J. Bec. "Finite-size effects in the dynamics of neutrally buoyant particles in turbulent flow." *Journal of Fluid Mechanics*. **651**, 81-91. (2010).
- B. P. B. Hoomans, J. A. M. Kuipers, W. J. Briels and W. P. M. van Swaaij. "Discrete particle simulation of bubble and slug formation in a two-dimensional gas-fluidised bed: A hard-sphere approach." *Chemical Engineering Science*. **51**, 99-118. (1996).
- P. J. Ireland, A. D. Bragg and L. R. Collins. "The effect of Reynolds number on inertial particle dynamics in isotropic turbulence. Part 1. Simulations without gravitational effects." *Journal of Fluid Mechanics*. **796**, 617-658. (2016).
- P. Kosinski and A. C. Hoffmann. "Extended hard-sphere model and collisions of cohesive particles." *Physical Review E*. **84**, 031303. (2011).
- J. W. Krozel. "Electrokinetic Interactions between Two Spheres: The Role of Surface Charge Transport in Coagulation." *Journal of Colloid and Interface Science*. **163**, 437-453. (1994).
- J. Kuerten and A. Vreman. "Can turbophoresis be predicted by large-eddy simulation?" *Physics of Fluids*. **17**, 011701. (2005).
- J. D. Kulick, J. R. Fessler and J. K. Eaton. "Particle response and turbulence modification in fully developed channel flow." *Journal of Fluid Mechanics*. **277**, 109-134. (1994).
- J. Kussin and M. Sommerfeld. "Experimental studies on particle behaviour and turbulence modification in horizontal channel flow with different wall roughness." *Experiments in Fluids*. **33**, 143-159. (2002).
- S. L ain, M. Sommerfeld and J. Kussin. "Experimental studies and modelling of four-way coupling in particle-laden horizontal channel flow." *International Journal of Heat and Fluid Flow*. **23**, 647-656. (2002).
- Y. Li, J. B. McLaughlin, K. Kontomaris and L. Portela. "Numerical simulation of particle-laden turbulent channel flow." *Physics of Fluids*. **13**, 2957-2967. (2001).
- F. Lucci, A. Ferrante and S. Elghobashi. "Is Stokes number an appropriate indicator for turbulence modulation by particles of Taylor-length-scale size?" *Physics of Fluids*. **23**, 025101. (2011).
- C. Marchioli and A. Soldati. "Mechanisms for particle transfer and segregation in a turbulent boundary layer." *Journal of Fluid Mechanics*. **468**, 283-315. (2002).
- C. Marchioli, A. Soldati, J. Kuerten, B. Arcen, A. Taniere, G. Goldensoph, K. Squires, M. Cargnelutti and L. Portela. "Statistics of particle dispersion in direct numerical simulations of wall-bounded turbulence: Results of an international collaborative benchmark test." *International Journal of Multiphase Flow*. **34**, 879-893. (2008).
- M. Maxey. "The motion of small spherical particles in a cellular flow field." *The Physics of Fluids*. **30**, 1915-1928. (1987).
- L. F. Mortimer, D. O. Njobuenwu and M. Fairweather. "Near-wall dynamics of inertial particles in dilute turbulent channel flows." *Physics of Fluids*. **31**, 063302. (2019).
- R. D. Moser, J. Kim and N. N. Mansour. "Direct numerical simulation of turbulent channel flow up to $Re_\tau=590$." *Physics of Fluids*. **11**, 943-945. (1999).
- D. O. Njobuenwu and M. Fairweather. "Deterministic modelling of particle agglomeration in turbulent flow." In: *Proceedings of the Eighth International Symposium on Turbulence, Heat and Mass Transfer*, New York: Begel House Inc., 587. (2015).
- D. O. Njobuenwu and M. Fairweather. "Simulation of deterministic energy-balance particle agglomeration in turbulent liquid-solid flows." *Physics of Fluids*. **29**, 083301. (2017).
- D. O. Njobuenwu and M. Fairweather. "Large eddy simulation of particle agglomeration with shear breakup in turbulent channel flow." *Physics of Fluids*. **30**, 063303. (2018).

- B. Oesterle and A. Petitjean. "Simulation of particle-to-particle interactions in gas solid flows." *International Journal of Multiphase Flow*. **19**, 199-211. (1993).
- Y. Pan and S. Banerjee. "Numerical simulation of particle interactions with wall turbulence." *Physics of Fluids*. **8**, 2733-2755. (1996).
- J. J. Riley and G. Patterson Jr. "Diffusion experiments with numerically integrated isotropic turbulence." *The Physics of Fluids*. **17**, 292-297. (1974).
- G. A. Roure and F. R. Cunha. "Hydrodynamic dispersion and aggregation induced by shear in non-Brownian magnetic suspensions." *Physics of Fluids*. **30**, 122002. (2018).
- K. C. J. Schutte, L. M. Portela, A. Twerda and R. A. W. M. Henkes. "Hydrodynamic Perspective on Asphaltene Agglomeration and Deposition." *Energy & Fuels*. **29**, 2754-2767. (2015).
- C. A. Shook and M. C. Roco. *Slurry Flow: Principles and Practice*. (Butterworth- Heinemann, Stoneham, 1991).
- M. Sommerfeld. "Validation of a stochastic Lagrangian modelling approach for inter-particle collisions in homogeneous isotropic turbulence." *International Journal of Multiphase Flow*. **27**, 1829-1858. (2001).
- K. D. Squires and J. K. Eaton. "Preferential concentration of particles by turbulence." *Physics of Fluids A: Fluid Dynamics*. **3**, 1169-1178. (1991).
- J. Tingey, B. Bunker, G. Graff, K. Keeper, A. Lea and D. Rector. "Colloidal agglomerates in tank sludge and their impact on waste processing." *MRS Online Proceedings Library Archive*. **556**, 1315. (1999).
- J. Tomas. "Adhesion of ultrafine particles—a micromechanical approach." *Chemical Engineering Science*. **62**, 1997-2010. (2007).
- N. Vdović and J. Bišćan. "Electrokinetics of natural and synthetic calcite suspensions." *Colloids and Surfaces A: Physicochemical and Engineering Aspects*. **137**, 7-14. (1998).
- A. W. Vreman and J. G. M. Kuerten. "Comparison of direct numerical simulation databases of turbulent channel flow at $Re_{\tau}=180$." *Physics of Fluids*. **26**, (2014).
- B. Vreman, B. J. Geurts, N. Deen, J. Kuipers and J. G. Kuerten. "Two-and four-way coupled Euler–Lagrangian large-eddy simulation of turbulent particle-laden channel flow." *Flow, Turbulence and Combustion*. **82**, 015102. (2009).
- J. Wang, Q. Shi, Z. Huang, Y. Gu, L. Musango and Y. Yang. "Experimental investigation of particle size effect on agglomeration behaviors in gas–solid fluidized beds." *Industrial & Engineering Chemistry Research*. **54**, 12177-12186. (2015).
- Y. Yamamoto, M. Potthoff, T. Tanaka, T. Kajishima and Y. Tsuji. "Large-eddy simulation of turbulent gas–particle flow in a vertical channel: effect of considering inter-particle collisions." *Journal of Fluid Mechanics*. **442**, 303-334. (2001).
- F. Zhao, W. George and B. Van Wachem. "Four-way coupled simulations of small particles in turbulent channel flow: The effects of particle shape and Stokes number." *Physics of Fluids*. **27**, 083301. (2015).